

**DESIGN AND EVALUATION OF LINEAR INTRACAVITARY ULTRASOUND
PHASED ARRAY FOR MRI-GUIDED PROSTATE ABLATIVE THERAPIES**

by

Shunmugavelu D. Sokka
Bachelor of Science, Biomedical Engineering & Electrical Engineering
Duke University, 1996

Submitted to the Department of Electrical Engineering and Computer Science in
partial fulfillment of the requirements for the degree of

**MASTER OF SCIENCE IN ELECTRICAL ENGINEERING AND COMPUTER
SCIENCE**

at the

MASSACHUSETTS INSTITUTE OF TECHNOLOGY

August 1999

[September 1999]


Copyright © Massachusetts Institute of Technology, 1999. All rights reserved.

Signature of
Author



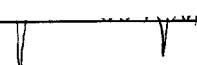
Shunmugavelu Sokka
Department of Electrical Engineering and Computer Science
August 24, 1999

Certified
by



Kullervo Hynynen, Ph.D.
Associate Professor of Radiology, Harvard Medical School
Thesis Advisor

Certified
by

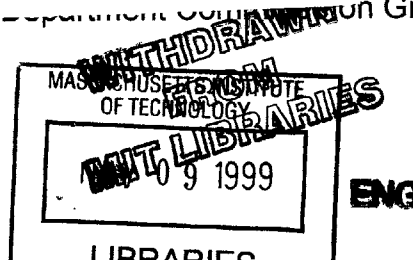


John L. Wyatt, Jr., Ph.D.
Professor of Electrical Engineering and Computer Science, M.I.T.
Departmental Advisor

Accepted
by



Chair, Department of Electrical Engineering and Computer Science
Graduate Theses



Design and Evaluation of Linear Intracavitary Ultrasound Phased Array for MRI-Guided Prostate Ablative Therapies

by
Shunmugavelu D. Sokka

Submitted to the Department of Electrical Engineering and Computer Science in Partial Fulfillment of the Requirements for the Degree of Master of Science in Electrical Engineering and Computer Science at the Massachusetts Institute of Technology
August, 1999

Abstract

Over the past decade, numerous minimally invasive thermal procedures have been investigated to treat benign prostate hyperplasia and prostate cancer. These hyperthermia and thermal surgery techniques have employed RF energy, microwave radiation, laser, and acoustic energy to heat and necrose a localized region of tissue. Of these methods, ultrasound has shown considerable promise due to its ability to produce more precise and deeper foci *in vivo*. In addition, recent advances in ultrasound amplifier and fabrication technologies have prompted refined clinical heating devices. In this study, a linear, transrectal, ultrasound phased array capable of ablating large tissue volumes was fabricated and evaluated in tissue. The device was designed to be MRI compatible for use with MRI thermometry and guidance. The intracavitary applicator increases treatable tissue volume by utilizing an ultrasonic motor to provide up to a 100-degree mechanical rotation angle to a 62-element 1D ultrasound array. An aperiodic array geometry was used to reduce grating lobes. The applicator built under constraints of the small rectal dimensions also incorporated a 1 mm thin custom-fabricated Kapton flexible circuit to interconnect the elements of the phased array to the ultrasound driving system. The Kapton interconnect reduced cable crosstalk and hence also improved the acoustic efficiency of the array. The array was driven by a multi-channel ultrasound amplifier system, which incorporates power and phase feedback circuitry to improve thermal focusing. MRI guided *in vivo* and *ex vivo* experiments were performed to verify the array's large volume ablative capabilities. *Ex vivo* bovine experiments were performed to assess the focusing range of applicator. The array generated foci in a 3 cm (2 to 5 cm from the array surface along the axis normal to the array) by 5.5 cm (along the long axis of the array) by 6 cm (along the transverse axis of the array at a depth of 4 cm) volume. Following *ex vivo* studies, *in vivo* rabbit thigh experiments were performed to evaluate the lesion producing capabilities in perfused tissue. The array generated 3 cm x 2 cm x 2 cm lesions with 8-12 half minute sonications equally spaced in the volume. The results indicate that transrectal ultrasound coagulation of the whole prostate is feasible with the method developed.

Thesis Advisor: Kullervo Hynynen, Ph.D.

Title: Associate Professor of Radiology, Harvard Medical School and Brigham and Women's Hospital.

ACKNOWLEDGMENTS

The author would like to thank Dr. Kullervo Hynynen for the opportunity to work on this project and for providing an ideal environment for research. His guidance, encouragement, accessibility for discussion, and most importantly his patience are much appreciated. The author would like to thank Todd Fjield, Doug Daum, and Mark Buchanan for their invaluable advice during the design and construction phase of the phased array system. The author is also appreciative of Nathan McDannold, Randy King, Heather Martin, and Nadine Smith for their help with MRI experiments.

The author would also like to thank other members of the research group at the Brigham & Women's Hospital: Dr. Greg Clement, Adan Ackerman, Tonia Gieske, Dr. Jie Sun, Dr. Ibrahim Hallaj, Dr. Peter Huber, Jon Thierman, and Dr. K. Kuroda. Their assistance in every area from transducer fabrication to thesis editing is appreciated. The author would like to thank: Tim Ritter and Pat Lopath at the Penn State Whitaker Center for Medical Ultrasonics for dicing the transducers, Joe Walsh at the Microsystems Technology Laboratory at M.I.T. for providing access to the gold wire bonder, and Matt Radamacher for machining the intracavitary applicator.

The author is appreciative of the NIH/NCI (Grant #R01CA48939), the M.I.T. Division of Health Science and Technology, and the Whitaker Foundation for providing funding for this project and his graduate education.

Most importantly, the author would like to thank his mother for providing unconditional support and his father for providing the inspiration for pursuing higher education. The author would like to dedicate this thesis to him.

TABLE OF CONTENTS

LIST OF FIGURES.....	7
LIST OF TABLES.....	8
1 INTRODUCTION	9
1.1 PROSTATE DISEASE	9
1.2 TREATMENTS.....	10
1.3 THERMAL THERAPIES FOR PROSTATE	12
1.4 FOCUSED ULTRASOUND SURGERY	14
1.4.1 <i>Advantages</i>	14
1.4.2 <i>Recent Advances</i>	15
1.5 OTHER PROSTATE ARRAY DESIGNS	19
1.6 SCOPE OF THIS THESIS	25
2 ULTRASOUND ARRAY FABRICATION.....	27
2.1 INTRODUCTION.....	27
2.1.1 <i>Array Requirements</i>	27
2.1.2 <i>Current State of Array Fabrication</i>	27
2.2 METHODS AND MATERIALS	30
2.2.1 <i>Test Array Construction</i>	30
2.2.2 <i>Acoustic Efficiency measurements</i>	35
2.2.3 <i>Maximum Power measurements</i>	35
2.2.4 <i>Coupling measurements</i>	36
2.3 RESULTS.....	36
2.3.1 <i>Ground Plane</i>	36
2.3.2 <i>Encapsulates</i>	38
2.4 DISCUSSION AND CONCLUSIONS	39
3 CONSTRUCTION OF PHASED ARRAY SYSTEM FOR TRANSRECTAL ABLATION.....	41
3.1 TRANSDUCER	41
3.2 INTRACAVITARY APPLICATOR	42
3.3 ASSEMBLY & OPERATION	48
3.4 AMPLIFIER.....	54
4 EVALUATION OF PHASED ARRAY IN <i>EX VIVO</i> AND <i>IN VIVO</i> TISSUES	55
4.1 INTRODUCTION.....	55
4.2 MATERIALS AND METHODS	55
4.2.1 <i>MRI Experimental Setup</i>	55
4.2.2 <i>MRI Imaging Techniques</i>	56
4.2.3 <i>Ultrasound Protocols</i>	58
4.3 RESULTS.....	59
4.3.1 <i>Ex Vivo Experiments</i>	59

4.3.2	<i>In Vivo Experiments</i>	64
4.4	DISCUSSION	71
4.4.1	<i>Ex vivo Bovine Phantom Experiments</i>	71
4.4.2	<i>In vivo Rabbit Thigh Experiments</i>	71
5	CONCLUSIONS	74
	REFERENCES	76

LIST OF FIGURES

Figure 1-1. Schematic of Cylindrical element transducer in a transrectal applicator.....	20
Figure 1-2. Diagram of an eight sector spherical-sectioned transducer.	23
Figure 1-3. Diagram of a linear phased array.....	24
Figure 2-1. Schematic showing test array construction at different stages (a-c).	31
Figure 3-1. Diagram showing the electrical focusing capabilities of the linear transducer.	42
Figure 3-2. Schematic of the intracavitary applicator	46
Figure 3-3. Close-up of the front portion of the intracavitary applicator.	47
Figure 3-4. Illustration of the array's rotation.	47
Figure 3-5. Pictures of the array at various stages of construction.	50
Figure 3-6. Cross-section of the applicator with mounted transducer.	53
Figure 3-7. Picture of the completed intracavitary applicator.	53
Figure 4-1. Diagram of experimental setup.	56
Figure 4-2. T1-weighted radial-transverse (RT) plane image of the bovine phantom setup.	60
Figure 4-3. AT-plane temperature images showing the phasing abilities of the array.	61
Figure 4-4. AT-plane (a), AR-plane (b), and RT-plane (c) temperature images of a 4 cm-deep focus generated by switching.	62
Figure 4-5. RT-plane temperature images showing the transverse focusing range of the array as it is mechanically rotated.	63
Figure 4-6. AR-plane temperature images acquired during a high power sonication (130 watts, 30 seconds).	65
Figure 4-7. Temperature profile along the 36 mm vertical distance shown in Figure 4-6a at the end of sonication	66
Figure 4-8. Temperature rise at the focus during sonication and during 25 seconds of the cooling time.	66
Figure 4-9. T2-weighted image after sonication and cooling.	67
Figure 4-10. Gross histology of treatment 2	69
Figure 4-11. T2-weighted images in the AT-plane (a) and in the AR-plane (b) after 8 sonications (130 watts, 30 seconds).....	70

LIST OF TABLES

Table 2-1. Efficiency, maximum power, and coupling measurements for different ground plane techniques	37
Table 2-2. Efficiency, maximum power and coupling measurements for different encapsulates	39
Table 4-1. Outcomes of the three ultrasound <i>in vivo</i> rabbit thigh treatments.	68

1 Introduction

1.1 Prostate Disease

Prostate Disease is among the leading causes of morbidity and mortality in the United States. In 1999, there will be an estimated 179,300 new cases of prostate cancer, making it the most frequently diagnosed cancer in the population (Landis et al. 1999). This year, 37,000 men will die from prostate carcinoma, second only to lung cancer in neoplasia related fatalities. While prostate cancer is a leading of cause mortality in the United States, benign prostatic hyperplasia (BPH) or prostatism is one of the leading causes of morbidity. Pathologically, BPH involves benign nodular hyperplasia of both the stromal and epithelial tissues within the prostate, leading to enlargement of the organ (Hollander and Diokno 1996). Studies have shown that 50% of all males in their fifties and 90% of males in their nineties exhibit some pathological evidence of BPH (Berry et al. 1994). This pathological condition leads to a wide variety of clinical manifestations, with urinary tract infection, retention, hematuria, and obstructive uropathy among them (Hollander and Diokno 1996). A quarter of all men aged 55 present with BPH-related urinary flow rate reduction. This number increases to 50% in men aged 75 (Arrighi et al. 1990). The high incidences of both prostate cancer and BPH have prompted a large amount of investigation in diagnosis and treatment of these diseases. For BPH, the majority of research is focused on treatment, as diagnosis of BPH is fairly straightforward. Prostate cancer, however, is a much more complicated

disorder. Diagnosis of prostate cancer is a continually evolving field plagued with problems of missed diagnoses, false positives, and understaging (Garnick and Fair 1996a). In 1994, the FDA approved the non-invasive prostate specific antigen (PSA) test which today is the subject of much debate as the low specificity test has led to numerous unnecessary biopsies and follow-up imaging. An equally alarming problem in prostate cancer diagnosis is understaging. Studies indicate that as many as 50% of patients who had initially been diagnosed with organ-confined disease showed histological evidence of metastatic diseases after initial treatment. Some of these shortfalls in prostate cancer diagnosis may be overcome if an optimal treatment for all stages of prostate carcinoma can be developed.

1.2 Treatments

Treatment modalities for BPH include pharmacological agents, transurethral resection, prostatectomy, hyperthermia, ablation, transurethral stents, and balloon dilation. Patients presenting with BPH are initially treated medically with agents such as finasteride which lower testosterone levels and thus cause the prostate to shrink in size. Long term studies with finasteride, the only FDA approved hormone related therapy, have shown poor efficacy. Although the drug has few side effects, a 5% impotence rate among them, it took some patients up to 12 months to respond and many never responded to treatment (Stoner 1994). If pharmacological treatments fail, transurethral resection of the prostate (TURP) is performed. TURP has long been the “gold

standard" treatment for BPH, yielding symptomatic improvements in 80 to 90% of the cases (Hollander and Diokno 1996). The procedure, however, has a high complication rate; studies indicate that rates vary from 18 to 33%.

Complications and side effects include postoperative hemorrhage, hyponatremia, post operative clot retention, urinary tract infection, urine retention, erectile dysfunction, and retrograde ejaculation. If problems persist after TURP, radical prostatectomy is performed as a definitive treatment for BPH, but the procedure is significantly more invasive and riskier than the other methods.

Treatments for prostate cancer include hormonal therapy, radiation therapy, radical prostatectomy, brachytherapy, and cryosurgery. Treatment is based on the cancer staging. Organ-confined tumors, classified as T1 or T2, are typically treated by radical prostatectomy alone or in conjunction with hormonal therapy while tumors that have spread beyond the prostate, classified as T3-T4, N, or M, are treated by some combination of radiation, hormonal and chemotherapies (Garnick and Fair 1998). All of these therapies have side effects. As high as 70% of patients that undergo radiation therapy and prostatectomy experience impotence, while 2-15% of patients experience mild to severe incontinence. Despite the high incidence of side effects, prostatectomy continues to be the definitive treatment for organ-confined prostate cancer as the treatment has the highest long-term survival rate, approximately 70% over 10 years (Frohmueller and Theiss 1995; Garnick and Fair 1996b). Although therapies for both BPH and prostate cancer are fairly well established, these therapies are by no means optimal. Patients with these prostate diseases would

benefit tremendously from the development of a more effective, safer, and less invasive treatment.

1.3 Thermal Therapies for Prostate

Among the many alternative therapies being investigated, thermal therapies of the prostate, such as hyperthermia and thermal ablation, show considerable promise. Hyperthermia refers to mildly heating localized regions of tissue (42-45°C) for a long duration (15-60 minutes). As a cancer treatment, hyperthermia has been shown to cause cell death directly (Dewey et al. 1977; Strobehn 1984) as well as indirectly by enhancing the cytotoxic effects of radiation therapy (Dewey et al. 1977; Overgaard 1989) and chemotherapy (Hahn 1979). For prostate hyperthermia, temperatures in the prostate volume (4-6 x 4 x 2 cm³) should be elevated 5-8°C while limiting the temperature elevation in the surrounding tissue to less than 5 degrees. Hyperthermia treatments have been investigated clinically and have shown promise for the treatment of both BPH (Stawarz et al. 1991) and prostate cancer (Strohmaier et al. 1991; Fosmire et al. 1993).

Thermal ablation, also referred to as thermal surgery, is used clinically to necrose both malignant and benign tissues. During ablation treatments, temperatures in a small localized region, typically 1-3 mm³, are elevated to 60-100°C for durations of 1 minute or less. Thermal ablation techniques have been studied for decades; studies from the mid 20th century have shown that focused ultrasound can create precise lesions without injury to surrounding tissue (Lynn

et al. 1942; Fry 1954). Thermal ablation can be used to treat BPH by necrosing tissue adjacent to the urethra to relieve urinary tract obstruction. Thermal surgery techniques can naturally be extended to treat prostate cancer. Tumors demarcated by imaging can be treated with precise focusing of thermal energy or the whole prostate can be necrosed, effectively performing a prostatectomy. This second therapy, thermal prostatectomy, would have an immediate impact on prostate disease management, as it would provide the definitive treatment for both BPH and non-metastatic prostate cancer without the complications and invasiveness associated with conventional surgery.

Several therapies employ electromagnetic energy to thermally ablate tissue in the prostate. The majority of these treatments are used to ablate small volumes of prostate tissue. The most common of these methods is TURP, which employs RF energy at roughly 240 watts to necrose tissue transurethrally. Transurethral electrovaporization is another technique that employs RF energy, but at higher powers to vaporize tissue (Vaportrode, Santa Barbara, CA). Studies with the Vaportrode have shown that BPH treatments can be done with fewer side effects and shorter operating times than TURP (Kaplan 1993). Lasers have also been investigated to treat BPH; transurethral ultrasound guided laser prostatectomy (TULIP) has been shown to be effective in necrosing the prostate tissue that immediately surrounds the urethra (Anson et al. 1993). Although the laser can be aimed accurately, urologists have difficulty visualizing the treated region. Microwaves have also been used to treat the prostate at both hyperthermia and thermal surgery temperature ranges. Transurethral

applicators designed for thermotherapy can focus energy into the prostate volume while reducing the discomfort associated with heating the prostatic mucosa. Studies with these devices have been shown to objectively improve urinary flow rates and other BPH symptoms (Devonec et al. 1993). Microwave hyperthermia applicators have been designed to provide uniform heating to larger volumes of the prostate. These microwave antennas are encased in transrectal applicators so that larger volumes of the prostate can be heated while reducing the urinary tract related complications associated with transurethral devices (Strohmaier et al. 1991; Stawarz et al. 1991). Microwave phased array antennas have sharpened the power deposition patterns (Short 1980; Diederich and Stauffer 1993) and increased the penetration depth (Hand 1986; Lee 1992) compared to conventional microwave antennas. However, even these refined antennas have problems with creating focused heating fields deeper than 3 cm at an operating frequency of 915 MHz (Fenn 1993). Although all of these electromagnetic therapies show promise for thermal treatments, electromagnetic waves lack the ability to focus thermal energy into deeper regions (>3 cm from the source) of tissue. As a result, their use has been restricted primarily to BPH treatment.

1.4 Focused Ultrasound Surgery

1.4.1 Advantages

Focused ultrasound surgery (FUS) utilizes high intensity focused ultrasound to cause coagulative necrosis in tissue. At therapeutic frequencies,

0.5 to 4 MHz, ultrasound can be tightly focused with little power deposition in the near field. A typical ultrasound wave at 1.0 MHz has a wavelength of 1.5 mm and a penetration depth of roughly 10 cm (Hynynen 1990) in soft tissue. In comparison, a microwave, which radiates at 2450 MHz has a wavelength of 1.8 cm and a penetration depth of only 1.7 cm in tissue (Johnson 1972).

Ultrasound has been investigated for treatment by several researchers in several organ systems, with breast, liver, prostate, and brain among others (Szent-Gorgyi 1933; Horvath 1944; Burov 1956a; Burov and Adreevskaya 1956b; Oka 1960; Lele 1975; Lele 1967; Fry and Johnson 1978; Frizzell et al. 1977; Vallancien et al. 1993; Sanghvi et al. 1996; ter Haar 1995; Crum and Hynynen 1996; Prat et al. 1995). Ultrasound can cause tissue necrosis via two methods: 1) thermal energy absorption and 2) the implosion of cavitation bubbles induced by higher pressure ultrasound waves. Although the cavitation mode shows potential (Hynynen et al. 1996b; Lele 1977; Prat et al. 1994; Sanghvi 1998), the thermal mode is better characterized as it yields lesion sizes and shapes predicted by models (Fan and Hynynen 1996; Damianou et al. 1995). In addition, therapy in the thermal regime is easily monitored with thermometry.

1.4.2 Recent Advances

As early as the 1930s, investigators, encouraged by the potential of X-ray therapy of cancers, explored ultrasound as a treatment modality (Szent-Gorgyi 1933; Nakahara and Kabayashi 1934; Horvath 1944; Lynn et al. 1942). These initial studies showed mixed results as some trials even demonstrated that

ultrasound induced cancer growth. These early studies and even the subsequent trials in the 1950s and 1960s that demonstrated the feasibility of ultrasound *in vivo* were limited technological in three main areas: image guidance, ultrasound transducers, and ultrasound driving systems.

Early ultrasound treatments lacked visual and thermal feedback, which made focusing the ultrasound at the desired location and monitoring thermal dose during treatment extremely difficult. These visualization techniques for both localizing the diseased tissue and then monitoring temperatures during treatment have evolved only recently. Several investigators have used ultrasonography for guidance (Fry 1968; Madersbacher et al. 1995; Sanghvi et al. 1999; Sheljaskov et al. 1997), but ultrasound thermometry is unreliable due to the speed of sound's dependence on temperature. Some have used CT for both focus localization and thermometry (Fallone et al. 1982; Jenne et al. 1997). However, MRI is the optimal imaging modality as both guidance and thermometry with high spatial and temporal resolution is possible. MRI provides excellent soft tissue contrast for diseased tissue segmentation, while temperature sensitive pulse sequences can be used to measure relative temperature changes with an accuracy of $\pm 0.5^{\circ}\text{C}$ (Ishihara et al. 1992; Chung et al. 1996; Samulski et al. 1992). Several studies have shown the feasibility of MRI-guided ultrasound surgery *in vivo* (Cline et al. 1995; Hynynen 1996a; Parker 1984; McDannold et al. 1998; Stepanow et al. 1995).

Therapeutic transducer technology has also evolved dramatically over the past two decades, mainly with the advent of phased array transducers. Ultrasonic phased arrays consist of multiple ultrasonic generators, piezoelectric elements, arranged in a specific geometry. The phase and amplitude of each generator is varied by the electronic driving system to shape the acoustic field. Phased arrays allow for beam steering. This provides a remarkable advantage over single element transducers, as foci can be moved by electronically varying the phase and amplitude of the driving signal. The higher field controllability afforded by phased arrays also allows for sidelobe reduction, minimizing the effects of secondary foci in the acoustic field. In many of the early FUS studies mentioned above, single element spherically curved transducers were used to geometrically focus ultrasound for ablation. With phased arrays, we are no longer limited to geometries that have fixed foci. For example, planar transducers can be phased to create different focal patterns. Phased arrays were first used in diagnostic transducers in the late 1960s and early 1970s for improved beam steering (Sommer 1968; Thurstone and von Ramm 1974). Although early studies suggested phased arrays would improve treatment (Lynn et al. 1942; Fry and Fry 1960), therapeutic phased arrays were not developed until the early 1980s when Do-Huu and Hartemann used phased arrays for localizing hyperthermia treatments (Do-Huu and Hartemann 1981). Their phased array applicator demonstrated that transducers diced into concentric rings could scan the focus along the axis of the transducer. Since then various investigators have developed arrays with different geometries for both focused ultrasound surgery

and hyperthermia. The original single element spherically curved transducer has been sliced and diced into different geometries, and linear, tapered, and other types of planar arrays have been developed to control different aspects of the acoustic field (Cain and Umemura 1986; Frizzell et al. 1985; Benkeser et al. 1987; Ocheltree et al. 1987; Ebbini et al. 1988; Fjield and Hynynen 1997; Hand et al. 1993).

The primary challenge associated with ultrasonic phased arrays is the difficulty in array construction; however, advances in array fabrication have made construction of these arrays more routine. Some of these advances are directly borrowed from the semiconductor and electronics industries. Tools for transducer dicing, critical for planar phased array construction, are the same tools used for wafer dicing in the semiconductor industry. Both diagnostic and therapeutic ultrasound have also benefited from the advances in the electronic interconnect industry. Kapton flexible interconnects are now used routinely to connect diagnostic transducers to the driving and receiving hardware.

Advancements in adhesive technologies have also influenced the rise of phased arrays. Improved epoxies, silicones, and polymers have helped preserve the structural integrity and water seal of the phased arrays' diced elements while reducing interelement coupling. Phased array construction has been further aided by piezocomposite transducer materials. Composite materials contain small piezoelements embedded in polymer. They can be molded into any shape and dimension. Instead of requiring dicing, the electrode layer of these materials can be etched away to create the elements of the phased array. This avoids the

need for precision cutting and adhesives. However, piezocomposite elements are less efficient than diced elements as piezocomposites have higher interelement coupling. Generating high powers with these elements is more difficult than in conventional diced phased arrays. Nevertheless, piezocomposite phased arrays have been successfully used to create lesions in porcine liver tissue (Daum and Hynynen 1998b).

1.5 Other Prostate Array Designs

Ultrasound arrays for treating prostate disease have evolved from unfocused transducers for hyperthermia to large-scale phased arrays for prostate ablation. Initial attempts at prostate disease treatment were done with unfocused transducers. One of the first systems used diced cylindrical elements in an intracavitary applicator for hyperthermia treatments (Diederich and Hynynen 1990). Fosmire et al. showed that these unfocused intracavitary arrays could be used clinically for treating prostate adenocarcinoma (Fosmire et al. 1993). These early attempts were limited by poor control of power deposition in the depth dimension. Because of this limitation, higher acoustic powers were needed to reach therapeutic temperatures. In a unfocused transrectal hyperthermia system it was found that for an applicator with cylindrical geometry (1.5 cm diameter) and frequency of 1.5 MHz, a minimum acoustic power/transducer length of 12 W/cm was needed to achieve hyperthermia temperatures (Hynynen 1990). Despite requiring large powers for efficacy, these first arrays did set a precedent for transrectal applicator design. Although

transurethral designs have been proposed (Diederich and Burdette 1996), most ultrasound prostate therapy transducers have been housed in intracavitary applicators. Intracavitary applicators bring the energy source close to the target volume, thereby minimizing normal tissue exposure. In addition, transrectal ultrasound delivery to the prostate is free of bone or air, both of which are barriers for ultrasound propagation.

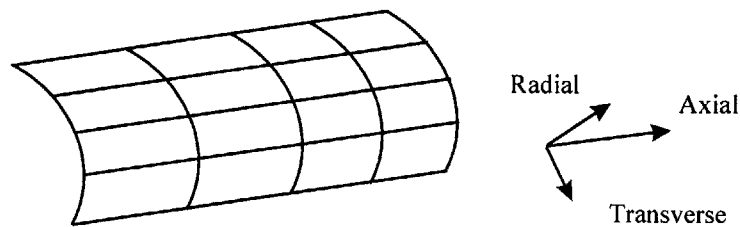


Figure 1-1. Schematic of Cylindrical element transducer in a transrectal applicator.

To combat poor power deposition in both the depth dimension and the axial dimension, phased arrays were proposed. In one study, a series of acoustic field/thermal simulations were performed to optimize element width ($\lambda/3$ to $5\lambda/3$ center-to-center), focus location (depth, center versus off axis), frequency (0.5 MHz to 2.0 MHz), and phased array length (3.75 cm to 10 cm) (Diederich and Hynynen 1991). From these simulations, a 40-cm long array with 180° cylindrical elements spaced 0.85λ center to center was constructed. While the array was not clinically suitable due to significant side lobe structure ($\sim 40\%$ power deposition) and short phased array length, it did show that electrical focusing of ultrasound into tissue 2 to 5 cm deep was feasible with an intracavitary array. Subsequent arrays attempted to reduce side lobe structure

by increasing the number the elements in the phased array. A 64 element cylindrical array with 0.58λ center to center spacing, 11.05 cm long, operating at 0.5 MHz was constructed (Buchanan and Hynynen 1994). This array performed better than previous attempts, but ~20% grating lobes still existed when focusing 2.5 cm off axis at 4 cm depth. In this study, focused ultrasound experiments were also performed. In *ex vivo* perfused kidney, the array was able to elevate temperature at the focus only 12°C, which is insufficient for ablative treatment.

While cylindrical elements conformed to the geometry of transrectal applicators and were adequate for hyperthermia, newer transducer geometries were needed to reduce grating lobes and to create the higher intensity focal patterns for ablation. To deliver higher powers at fixed focal distance, spherical-sectioned arrays were developed for transrectal treatment of the prostate. These transducers were able to successfully ablate human prostate (Madersbacher et al. 1994) tissue producing 10 mm lesions at fixed distances from the array. And in perhaps the largest multi-site clinical trial for ultrasound BPH treatment, transrectal spherical-sectioned arrays of varying focal length, 2.5 to 4.5 cm, were used to treat benign prostatic hyperplasia (Sanghvi et al. 1999). In the study, a rectangular 30 x 22 mm cut-out from a spherical transducer operating at 4 MHz was used for therapy and imaging. The transducer is divided in two with a center 11 mm circular segment used for pulse-echo imaging, and an outer annulus which is used in conjunction with the center segment for focused ultrasound treatment. The transducer housed in the intracavitary applicator can be

mechanically translated and rotated along the axis for greater prostate volume coverage. However, different arrays with different focal lengths are needed to move the focus in the depth dimension. Almost all of the 62 patients in the study showed significant improvements in peak urinary flow rate, International Prostate Symptom Scores (IPSS), and quality of life scores (QOL) over a 2 year period with few complications and no injury or side effects. The treatment is a safe and durable alternative to TURP for BPH, but ablating large prostate volumes for prostate cancer treatment is not feasible with this array. Secondly, the fixed focus transducer can only be used for ablation, and cannot be used for hyperthermia.

Fixed focus transducers have also been used in transrectal prostate cancer treatments (Gelet et al. 1999). In this study, 50 patients were treated for localized prostate cancer. The treated patients were followed for a median of 24 months, and based on PSA levels and sextant biopsy results, 56% of patients were in complete remission. The remainder of the patients were grouped into 3 groups: patients who failed the PSA test (6%), patients who had positive biopsies(18%), and patients who failed both tests on follow-up (20%). The problem with treating localized prostate cancer is previously discussed understaging issue. Too often, the degree of prostate cancer is underestimated, so local ultrasound ablation might not treat all neoplastic regions. Patients who were diagnosed with localized prostate cancer could have had cancer nodes in other areas of the prostate. Although the study shows that focused ultrasound could be used to treat prostate cancer with minimal side effects, the results

indicate that treating localized prostate cancer with fixed focus transducers is not the optimal approach for treating prostate cancer.

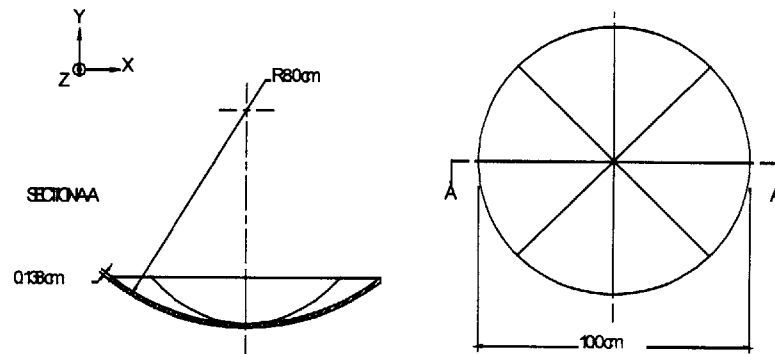


Figure 1-2. Diagram of an eight sector spherical-sectioned transducer.

Linear planar arrays were proposed as an another alternative (Hand et al. 1993). Prototype planar arrays for prostate therapy have been fabricated and tested in phantoms (Bechtold et al. 1997). This array geometry has advantages over both cylindrical-sectioned and spherical-sectioned arrays. Compared with cylindrical arrays, linear arrays do not have the $1/r$ acoustic intensity loss, and their heating fields do not increase in cross-sectional area as radial distance from the array increases. Linear arrays trade off the high gain natural focus of spherical-sectioned arrays for the ability to electronically move the focus. Thus, these arrays need to be driven at higher powers for equivalent thermal dose. Critical to the generation of high intensity foci is minimization of grating lobe structure. Linear phased antenna theory, developed initially for radar phased arrays, states that a linear array with a regular center-to-center spacing of $\lambda/2$ or less is perfectly steerable with no grating lobes along the axial and radial dimensions of the array. In ultrasound phased arrays, this geometry would

require elements on the order of 0.5 mm in width for 1.5 MHz transducers. Smaller elements mean increased difficulty in array construction, specifically in wiring and sealing. In addition, more elements would be needed to cover the same tissue volume, which would impose greater demands on the ultrasound driving system requiring more amplifier channels and phase shifters. Another disadvantage is that acoustic efficiency, the ratio of output acoustic power to input electrical power, decreases as element width decreases (Hynynen 1994).

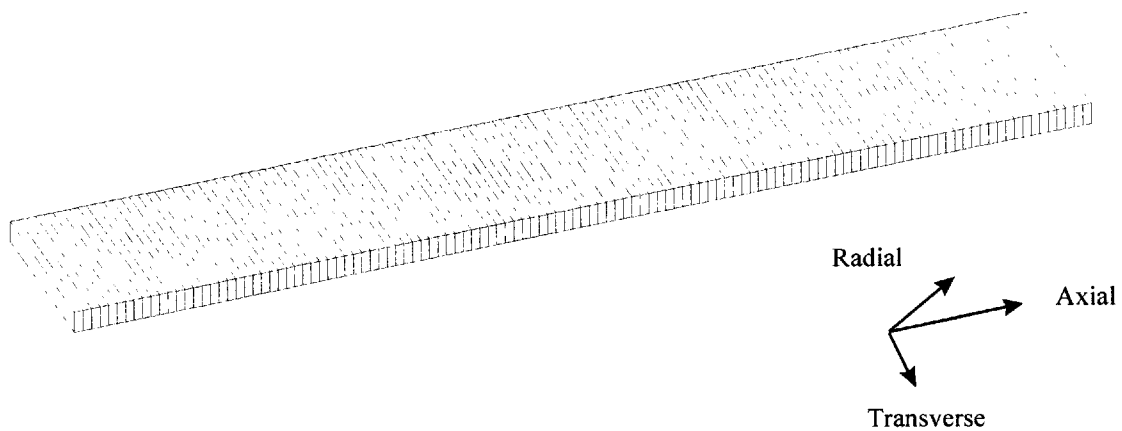


Figure 1-3. Diagram of a linear phased array.

For these reasons, irregular linear geometries have been investigated. Center-to-center spacing greater than $\lambda/2$ can be used if array periodicity is eliminated (Skolnik 1980). An extensive simulation study of aperiodic, tapered, and sparse linear geometries has shown that aperiodic arrays produce the lowest grating lobe levels (Hutchinson 1997). An optimal 57 element aperiodic array with two different element widths ordered randomly was fabricated and evaluated (Hutchinson et al. 1996). The array's two different element widths, array length, and element ordering were determined from a cost function

analysis, which favored geometries with low grating lobe levels. The fabricated array demonstrated that grating lobe levels can be reduced 30%-45% as compared to periodic arrays and that the average element width can be increased (20%-35%) over their periodic counterparts without an increase in grating lobe levels. In a subsequent study, a 62 element aperiodic array was incorporated into an intracavitary applicator, and *in vivo* and *ex vivo* experiments were performed with MRI thermometry (Hutchinson and Hynynen 1998). The study showed that small 4 mm x 4 mm x 7mm lesions could be created in *in vivo* rabbit thigh muscle and that MRI compatible intracavitary planar arrays could be used for ablation. However, since the Hutchinson array is linear, the focus can only be steered in 2 dimensions, along the radial and axial axes. The inability to move the focus in the transverse direction makes complete coverage of the prostate volume difficult.

1.6 Scope of This Thesis

In order for focused ultrasound surgery to become an accepted treatment method for prostate cancer, ultrasound arrays that can ablate large prostate volumes need to be developed. The primary goal of this research was to develop and test an intracavitary ultrasound phased array capable of whole prostate ablation. The study was conducted in series of three steps.

In the first portion of this study, phased array fabrication and manufacturing techniques were investigated. Current techniques are such that array reliability and power output are not adequate for clinical treatments. Various transducer

interconnect methods, wire bonding, Kapton printed circuits, and soldering schemes, were evaluated to reduce interelement crosstalk and to improve power output. In addition, alternative grounding techniques were investigated as poor grounding schemes have plagued phased arrays. Leaking of water into the back compartment of the transducer has also been a problem, so water sealing methods were also studied.

Then, with the optimal fabrication techniques, the intracavitary phased array was constructed. PZT-4 transducer material was diced to the Hutchinson 62 element aperiodic linear geometry to minimize grating lobes. The phased array transducer was housed in a transrectal applicator, which utilizes an ultrasonic motor to provide up to a 100-degree mechanical rotation angle to the 1D transducer array. The rotation axis provides a mechanical means of scanning the focus in the transverse direction, thus allowing complete 3D scanning of the high intensity focus. The complete device was also designed to be MRI compatible for use with MRI thermometry and guidance. The array was driven by a multi-channel ultrasound amplifier system with power and phase feedback circuitry designed to improve thermal focusing.

In the final portion of the study, MRI guided *in vivo* and *ex vivo* experiments were performed to verify the array's large volume ablative capabilities. Experiments in *ex vivo* bovine phantom were used to evaluate the volume extents of the arrays focusing capabilities. *In vivo* rabbit thigh experiments were used to test the array's ability to create large lesions in short treatment times.

2 Ultrasound Array Fabrication and Array Materials

2.1 *Introduction*

2.1.1 Array Requirements

One facet of this study was to improve upon the current materials and manufacturing techniques used in creating linear ultrasound phased arrays for thermal therapy. The basic requirements of these arrays are as follows. The array must be capable of delivering high acoustic powers, approximately 50-60 watts, reliably without sustained damage to the transducer or the applicator. Second, inter-element electrical and mechanical coupling must be minimized. Third, the arrays must be able to withstand prolonged submersion in water as this is the medium that couples the transducer to the tissue. Fourth, the array should be MRI compatible, so that treatment can be done with MRI guidance and thermometry. This section of the thesis will discuss the materials and manufacturing techniques investigated to meet these transducer requirements.

2.1.2 Current State of Array Fabrication

One dimensional phased arrays for therapeutic ultrasound are usually developed from a single rectangular PZT(Lead Zirconate Titanate) piezoelement. The PZT pieces are sputtered with a thin silver, copper, or gold electrode layer to provide a means for electric field application. Typically, these stock pieces are diced into the desired geometry, and the spaces between the elements (kerfs) are filled with silicones, epoxies, or other polymers. The filler material is selected

to minimize mechanical and electrical coupling between elements while maintaining the structural integrity of the phased array transducer. Once the transducer is diced, filled, and mounted into a frame, electrical connections to the elements of the phased array are made. Ground connections are made on the transmission side of the transducer and the high voltage signal lines are connected on the back face to minimize patient exposure to high electrical currents. Therapeutic transducers must transmit high levels of power for extended periods of time. For these reasons, the piezoelements are backed with a low impedance media on the back face to minimize backward transmission and sometimes coated with a quarter wave acoustic matching layer on the transmission side to minimize reflections in the forward direction. Air makes an ideal backing for therapeutic transducers as it eliminates backward transmission without increasing inter-element coupling (Wells 1977; Hynynen 1990). Continuous matching layers, on the other hand, increase inter-element coupling, and for many array geometries, they are avoided as the disadvantage of increased coupling outweighs any gains from the matching layer.

High demands are also placed on the electrical connections of therapeutic transducers. These connections must be able to handle large RF currents and voltages on the order of amps and hundreds of volts with minimal loss and must not transmit noise to or pick up noise from the MRI system. In addition, electrical interconnects should not contain iron based materials, and must minimize the amount of metal overall as MRI images are susceptible to metal artifacts. And, from a handling and construction perspective, the wire diameters

and interconnect dimensions should be small. Currently available micro coaxial cable satisfies these criteria, and a large variety of coaxial cables have been tested for use in therapeutic arrays (Daum 1998).

The Hutchinson array represents the state of the art in therapeutic linear phased arrays; many of the materials and manufacturing techniques mentioned above were used in this array (Hutchinson and Hynynen 1998). Extensive tests of filling adhesives were performed for this array (Daum 1998). The silicone (VI-SIL V-1022) used in filling this array performed well in high power, water immersion, coupling, and adhesion force tests. The entire array assembly, consisting of transducer, cables, and array holder, was MRI compatible. The array was also able to deliver the powers needed for ablation of the prostate, up to 180 watts of electrical power with acoustic efficiencies in the mid 40% range. However, at sustained high powers, the array leaked water, and the ground plane integrity was compromised. Water in the back of the transducer eliminates the low impedance air-backing and also increases the electrical coupling as the water provides a medium for crosstalk between the signal lines. In addition, wiring of the array in the transrectal applicator was extremely difficult. The wiring for 62 phased array elements was packed in a semi-circular area with a radius of 1 cm. The packaging of wires in this small area also increased the crosstalk between signal lines to the phased array element.

2.2 Methods and Materials

2.2.1 Test Array Construction

A series of 8-10 element test arrays were constructed to address the material and manufacturing shortfalls of the Hutchinson array: grounding, waterproofing, and wiring. Each test array was fabricated from 1.1 MHz PZT-4 pieces (EDO EC-69, Salt Lake City, UT). To match the element sizes of the proposed array, rectangular PZT pieces were diced into 15 mm X 1 mm and 15 x 1.15 mm elements with kerf size of 0.11 mm (NIH Transducer Resource Center, Penn State University, PA). Before dicing, the PZT stock piece was fixed onto a glass surface with either wax or Nitto tape. Kapton tape (3M, St. Paul, MN) is attached on the exposed surface to protect the electrode surface during the later filling phase. Then, the PZT was diced all the way through to the wax or Nitto tape with a diamond-impregnated blade mounted on a wafer dicing saw (K & S 782).

Once the PZT is diced, the kerfs were filled with degassed two-part (50:1) VI-SIL V-1022 silicone (Loctite Corp.). The silicone was poured onto the Kapton protected surface and kneaded into the kerfs. Each test array was then mounted in a polycarbonate frame with V-1022 silicone. After the silicone cured, typically 24 hours, the Kapton tape was removed to expose the electrode surface, and the surface was cleaned with steel wool (Figure 2-1a). Then, the electrical connections were made to the transducer, and the different sections of the

polycarbonate housing were glued together with RTV-108 (General Electric Silicones, Waterford, NY) to maintain a hermetic seal (Figure 2-1).

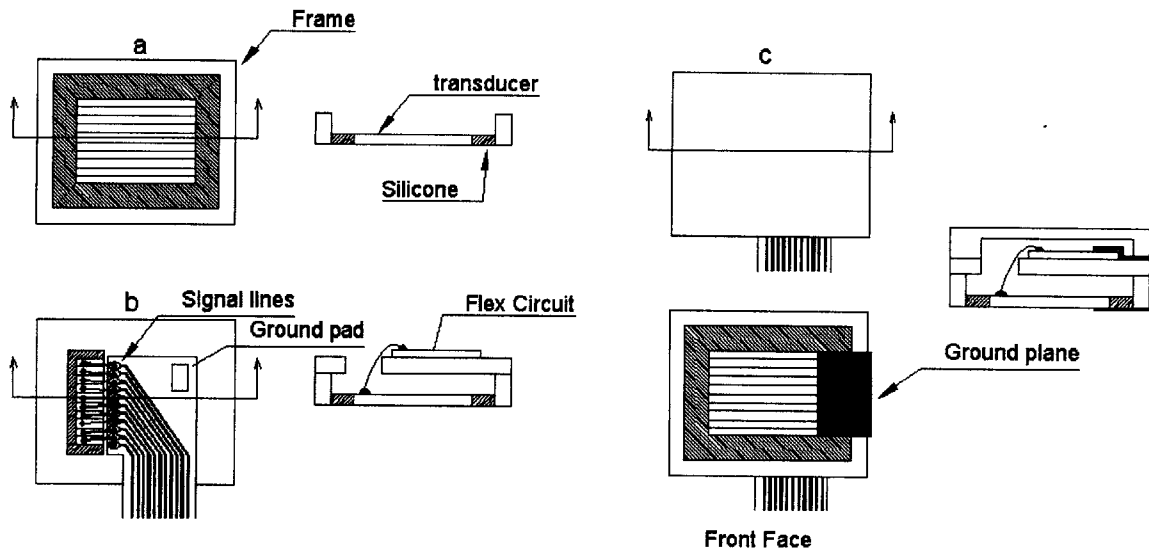


Figure 2-1. Schematic showing test array construction at different stages (a-c). The schematics show the back face and the side cross-sectional views of the test array at each stage. The flex circuit is shown in (b). The front face is also shown for the completed test array (c).

2.2.1.1 Kapton Flexible Circuit Interconnect

To address the wiring issues, a Kapton flexible interconnect was developed. There are multiple advantages to utilizing flexible printed circuit interconnects. First, a high density of wires can be packaged into a very small area. Second, printed circuits reduce signal line crosstalk, and circuits can be designed to handle large currents and voltages. In addition, the flexible interconnect makes the task of wiring easier. The interconnect was designed with three main criteria: 1) all signal lines must be able to handle up to 500 V_{p-p}

without breaking down 2) all lines must sustain currents up to 25 mA rms ; 3) the interconnect must have a cross sectional area no larger than a 5 mm radius semicircle. Based on these criteria, an 11-line flexible printed circuit with a ground plane was fabricated (Advanced Electronics, Minneapolis, MN). The signal lines were made with 2 ounce copper, and the interconnect has cross-sectional dimensions of 8 mm X 0.2 mm. All solder pads were gold plated to provide an optimal surface for soldering or gold wire bonding. Multiple flexible circuits could be layered to provide connections for additional elements.

The flexible circuit was mounted to the transducer frame and connected to the transducer elements with standard 30 AWG wire-wrap wire via soldering (Figure 2-1b). Gold wire bonding was investigated as a method for connecting transducer elements to the Kapton interconnect, but the 1 mil and 3 mil diameter wires tested were too brittle. In addition, gold wire bonds adhered well to the gold plated electrode of the flex circuit, but connected poorly to the silver electrode on the transducer. Silver wire bonding was also attempted, but again these wires were weak and adhered poorly to the silver electrode of the transducer. For these reasons, transducer elements were soldered to the flex circuit rather than gold wire bonded. Soldering was done at 550 °F, below the Curie temperature of the PZT piezoelements. Low capacitance micro-coaxial cables (32 AWG, Precision Interconnect, Portland, OR) were soldered to the other end of the flex circuit to provide an extended 7 meter cable assembly to the ultrasound amplifier system. The cable assembly was interfaced to the driving

system through a DL connector (ITT-Cannon, White Plains, NY) which was chosen to minimize cable reflections.

2.2.1.2 Ground Plane

Grounding the elements of transducers has historically been a problem in phased arrays with numerous small elements. When grounding small elements, the major issue is providing a solid ground plane without mechanically coupling the elements of the transducer. In the Hutchinson array, two grounding techniques were used: 1) the transducer was diced 85% through, and so all the elements were grounded through the intact face; 2) each element was individually soldered to ground. In the first technique, the 15% undiced PZT segments cracked at high powers. The soldered wire technique was rejected because it was not durable over a series of experiments.

In this study, test arrays were used to evaluate different grounding techniques. In all the test arrays, thin planar silver sheets were attached to front face covering only a small portion of the transducer face (Figure 2-1c). The silver sheet was passed through the transducer housing and soldered to the ground pad of the flex circuit. Three different ground plane techniques were tested. In one test array, silver conductive tape (3M, St. Paul, MN), was attached to the front face. In other arrays, conductive epoxies (Mereco Medaduct 1202, West Warwick, RI, and Tra-con, Bipax, Medford, MA) were used to attach silver foil (0.025mm thickness, Aldrich Chemical, Milwaukee, WI) to the transducer ground electrodes. Soldering of silver foil directly to the transducer

electrodes was also tested. In this technique, the silver foil was pre-tinned with a very thin layer of solder using solder flux. The foil was attached to the transducer ground electrodes by pressing the foil to the electrodes with the hot soldering iron. This created a very thin and strong connection between the ground electrodes and the silver foil. Test arrays with all ground plane methods were fabricated, and acoustic efficiency, maximum power, and coupling tests were performed to gauge the performance of the different grounding techniques.

2.2.1.3 Water Sealing

As discussed previously, water leaking to the back of transducer has been a problem in previous large-scale phased arrays. Water can leak in through gaps in the housing, through the silver foil or flex circuit exit slots, or through the kerfs in between the transducer elements. Leaking can become a more significant problem at high powers. When the transducer elements are vibrating at high amplitudes, negative pressure builds in the rear chamber of the transducer housing. This aids in pulling water in from the coupling bath, and water tends to collect even when only a minute leak is present. A wide variety of silicones, epoxies, and polymers (VI-SIL V-1022, RTV-108, Goop, & polyurethane glues) can be used to seal the gaps in the housing or gaps in the exit ports of ground plane and flex circuit, but leaking through the kerfs is a more complicated issue. To fix this problem, epoxy encapsulates were tested. The transmission face of each test array was coated with encapsulates to protect kerfs from water. Prior to the application of epoxy, the transducer face was cleaned thoroughly with

xylof and steel wool. Then, care was taken to apply a very thin layer of epoxy to the transducer face. Three epoxies were tested, Mereco 1650, Mereco 1670, and Mereco 401ST (West Warwick, RI). These epoxies had been used to coat other ultrasound transducers. Acoustic efficiency, maximum power, and coupling tests were performed with all three materials to verify the encapsulates' effect on ultrasound transmission.

2.2.2 Acoustic Efficiency measurements

Acoustic efficiency is the ratio of input electrical power to output acoustic power. The transducers were driven with a custom designed ultrasound amplifier system (Daum et al. 1998a) or an ENI power amplifier (ENI, Rochester, NY). The acoustic power measurements were made using a radiation force technique (Stewart 1982). The electrical power measurements for individual array elements were made using either a HP 438A Power Meter (Hewlett Packard, Englewood, CO) or the custom built power meters on the ultrasound driving system. Efficiency measurements for powering the entire array simultaneously used the custom-built power meters for each individual element attached to the driving system.

2.2.3 Maximum Power measurements

The maximum acoustic power was measured by progressively increasing the electrical power to an array element and measuring the acoustic output power until acoustic efficiencies began to drop more than 10%. Thus, maximum power recorded in the tables below is maximum sustainable power per element.

Efficiency measurements were again recorded at lower powers to measure the effect of high powers on the transducer elements. Peak power measurements were performed on all arrays that didn't fail in prior testing.

2.2.4 Coupling measurements

Inter-element coupling was tested by measuring the acoustic efficiency when adjacent array elements were electrically driven in-phase and out-of-phase. For in-phase measurements, all elements of the transducer were powered in phase with the custom-built amplifiers. For out-of-phase measurement, every element was driven 180° out of phase with its neighbor. Acoustic efficiency measurements for the whole array were made as described in the section above. The difference in the in-phase and out-of-phase efficiency measurements gives a measure of the inter-element coupling. Coupling measurements were performed on test arrays that had high acoustic efficiencies.

2.3 Results

2.3.1 Ground Plane

Table 2-1 shows the acoustic efficiency, maximum power measurements, and coupling measurements for the different grounding techniques evaluated in this study. Data from the Hutchinson array is provided to gauge the level of improvement in each of the different construction techniques. All the test arrays used to evaluate the grounding techniques, except those using silver tape, incorporated the Kapton flexible interconnect. The silver tape arrays used the same wiring scheme as the Hutchinson array: 30 AWG wire soldered to the

elements which were then soldered to coaxial cable to provide the 7 meter extension. In all cases, element acoustic efficiencies represent an average value for all tested elements near maximum acoustic powers. Maximum power measurements listed are values just prior to failure. Failure modes varied for the different arrays. The silver tape array and both silver epoxy test arrays failed due to ground plane detachment. In the soldered ground plane case, the elements probably failed due to depoling; there was no evidence of electrode detachment, arcing, or element cracking. In the two better forming grounding techniques, coupling measurements were performed in mid power ranges, not at the maximum power levels. In both cases, the out-of phase acoustic efficiencies were 9% lower than then the in-phase measurements, yet the out-of-phase coupling was still on par with the in-phase measurements of the Hutchinson array.

Table 2-1. Efficiency, maximum power, and coupling measurements for different ground plane techniques

Grounding Technique	Element Acoustic Efficiency	Maximum Acoustic Power per element	Inter-Element Coupling	
			In	Out
Hutchinson Array	46%	3.5 watts	42%	41%*
Silver Tape on edge	Failure			
Silver Tape on whole surface	15%	300 milliwatts		
Tra-con Bipax	27%	1.1 watts		
Mereco 1202	49%	3.6 watts	51%	42%
Soldering	60%	11.4 watts	58%	49%

*The out-of-phase measurement in the Hutchinson array is with the array focused at 5 cm distance radial to the array.

2.3.2 Encapsulates

Table 2-2 shows acoustic efficiency, maximum power measurements, and coupling measurements for the encapsulates evaluated in this study. In all the encapsulated test arrays, the soldering grounding technique was used. Results varied greatly depending upon the level of epoxy degassing, transducer face cleaning, and the thickness of the encapsulate layer. The data in the table shows the best results for each encapsulate. As with the grounding technique data, element acoustic efficiencies are averages over all tested elements near maximum powers. Maximum acoustic power measurements were made in 2-3 elements of the test array. Elements encapsulated with Mereco1650 showed a dramatic drop in acoustic efficiency just beyond the peak acoustic power recorded in the table. In the case of the Mereco1670, failure was due to detachment of the epoxy coating from the transducer face. In the Mereco 401ST test array, the elements would begin to overheat at peak acoustic power and the efficiency levels would drop below 10%. The power value just prior to the drop is listed in the table. Overheating did not cause damage to the elements as returning to lower power levels would yield efficiency measurements recorded earlier. Coupling measurements were done on the two better performing encapsulated test arrays. In both cases, in-phase and out-of-phase acoustic efficiencies differed by 8%; however, whole array efficiencies in the Mereco 1650 and 401ST were 10% and 13% (Table 2-2) lower respectively than the non-encapsulated case (Table 2-1).

Table 2-2 . Efficiency, maximum power and coupling measurements for different encapsulates

Encapsulate	Element Acoustic Efficiency	Maximum Acoustic Power per element	Inter-element Coupling	
			In	Out
Mereco 1650	55%	7.4	48%	40%
Mereco 1670	17%	0.5	20%	
Mereco 401ST	48%	1.2	45%	37%

2.4 Discussion and Conclusions

The test array data shows clear improvements in array performance with the new wiring and grounding techniques. Test arrays utilizing the Kapton flexible interconnect and the soldering grounding technique performed significantly better than the Hutchinson array in all categories, efficiency, maximum power, and inter-element coupling. Test arrays incorporating Mereco 1202 silver epoxy and the flexible circuit performed better or on par with the Hutchinson array in the test categories. The two most significant improvements with these techniques are the maximum power and whole array out-of-phase efficiency measurements. The maximum power measurements show that elements with solder and flex circuit connections can be driven up to 3.5 times harder without failure due to depoling or weakness in electrical interconnects. In addition, acoustic efficiencies of these elements when phased are better than the unphased efficiencies of the Hutchinson array. The Kapton printed circuit has more than likely reduced crosstalk between the signal lines. For these reasons,

both the soldering grounding technique and the flexible interconnect will be used in the construction of the 62-element phased array.

The encapsulate data suggests that Mereco 1650 can be used to seal the transmission face of the transducer without significant loss in performance. The 1650 epoxy, a flexible encapsulate, performed significantly better than the 1670, a fast curing flexible epoxy, and the 401ST, a stiffer, harder epoxy. The 1650 encapsulated array also was on par or better than the Hutchinson array in all tested categories. In addition to the water sealing abilities of these coatings, the encapsulates also act as an electrical insulation layer confining potentially dangerous leakage currents to the face of the transducer and not into the coupling media. The problem with these encapsulates, however, is that test arrays with the same coating had different test results. Consistency with the coating technique was not established. Furthermore, the best encapsulated arrays had acoustic efficiencies equal to the Hutchinson array, so encapsulating negated some of the improvements gained with the new fabrication techniques. Therefore, the 62-element phased array was not coated with any encapsulates. If leaking through the kerfs becomes a problem later on and if coating technique consistency improves, the 62-element phased array could be coated with Mereco1650.

3 Construction of Phased Array System for Transrectal Ablation

The major focus of this thesis was the design and construction of an intracavitary phased array for transrectal ultrasound ablation. Using the techniques described in the previous section, a 62-element phased array was incorporated into a transrectal applicator capable of rotating the linear array along its long axis.

3.1 Transducer

The 62 element linear phased array was constructed from 1.1 MHz resonant PZT-4 (EDO EC-69) with the dice and fill technique detailed in the previous section. The array incorporates 31 1.0 x 15 mm elements and 31 1.15 x 15 mm elements that are randomly ordered (with total dimensions of 15 mm x 75 mm). The particular aperiodic geometry, i.e. the ordering, used in this array comes from a previous simulation and optimization study that showed significant reduction in grating lobe structure with aperiodic linear geometries (Hutchinson 1997). Acoustic simulations of this array geometry demonstrated that foci with minimal lobe structure can be generated in a 3 cm x 6 cm area 3 cm from the array surface (Figure 3-1).

High intensity foci are produced by electrically setting the phases of each element so that constructive interference of the pressure waves from each element occurs at the desired focal position. The required phase for each

element is calculated using the differences in path length from the center of each element to the desired focus:

$$\phi_i = \frac{360}{\lambda}(d_i - d_0) - 360n \quad (3-1)$$

where ϕ_i is the phase of element i in degrees, d_i is the distance from the center of element i to the desired focus, d_0 is the distance from the center of the reference element to the focus, i is the element number ranging from 1 to 62, and n is an integer used to keep ϕ_i between 0° and 360° (Figure 3-1).

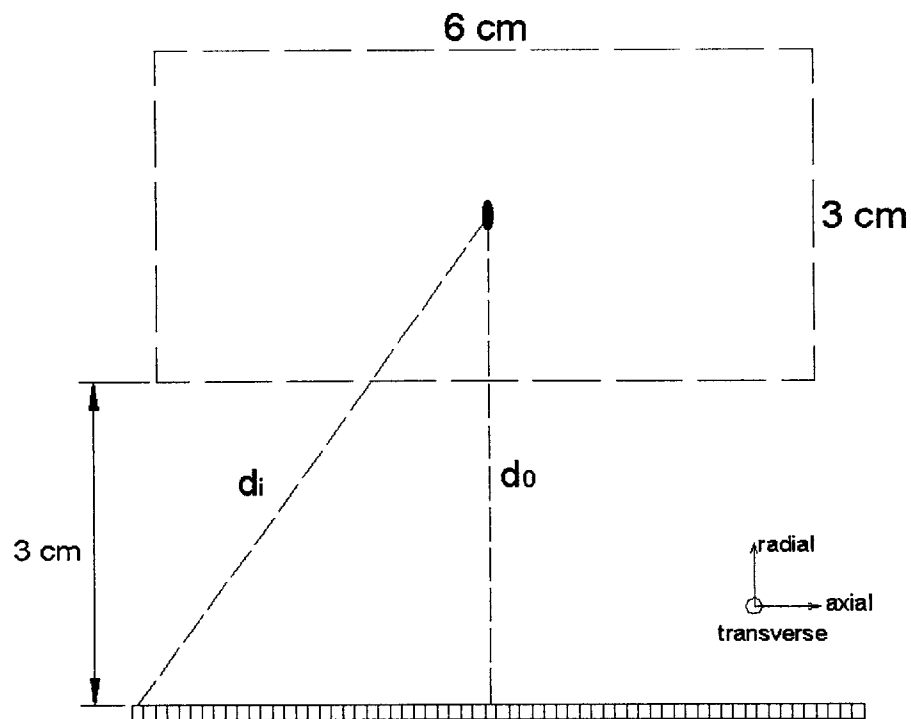


Figure 3-1. Diagram showing the electrical focusing capabilities of the linear transducer. The phased array can focus ultrasound in a 3 cm X 6 cm area 3 cm from the transducer surface.

3.2 Intracavitary Applicator

The linear phased array transducer was incorporated into an intracavitary applicator suitable for transrectal use. The applicator was designed to satisfy

several criteria. First, due to anatomical constraints, the portion of the applicator that must be in the rectum was designed to be as small as possible yet large enough to house the transducer and its wiring. Second, the applicator was designed to be MRI compatible, so no ferromagnetic materials were used. The amount of non-ferromagnetic metals was also minimized since they can distort the MR images. The applicator was constructed from polycarbonate and acrylic, and nylon screws and polymer adhesives were used in assembly. The motor used for transducer rotation is MRI compatible. The design also incorporates an ultrasound coupling system. The rectal portion of the applicator has O-ring slots at both ends and water inlet and outlet lines so that a latex condom can be attached and filled with water to couple the transducer to the rectal wall and the underlying tissue. The circulation lines also allow temperature control of the water bolus. The design includes leak prevention measures. Air is circulated behind the transducer to provide small positive pressures. The circulation prevents leaking by counteracting the negative pressures created during sonication.

Figure 3-2 below shows a detailed schematic of the transrectal applicator. The dimensions are in millimeters. The basic design involves an inner cylinder that rotates within the outer housing. The transducer/frame assembly is mounted in the inner cylinder. The outer housing at the front portion (the portion placed in the rectum) of the applicator holds the latex condom and allows the transducer to rotate freely without contacting the rectal wall. The inner cylinder is coupled to the motor at the far end of the applicator. The flexible interconnect traverses the

length of the applicator from the rectum portion to the rear compartment where it is soldered to the 7-meter micro-coaxial cable (Precision Interconnect) extension. Water seals were placed at the entry to the rear compartment to prevent water from entering the rear chamber.

Figure 3-3 shows a close-up of the three components that comprise the front portion of the applicator: the transducer frame, the inner cylinder, and the outer housing. This section of the applicator is 21 mm in diameter and 105 mm long. The outer housing's primary function is to anchor the latex condom; therefore, condom securing O-ring slots were fabricated into the outer housing. The inner cylinder serves as the transducer's mounting bed. It also houses the water lines and all the wiring. The inner diameter of the inner cylinder is 13 mm, which is large enough to accommodate the flexible interconnect and the water lines. Figure 3-4 shows the rotation of the inner cylinder within the outer housing. The transducer can be rotated 50° in both the clockwise and counterclockwise directions.

An ultrasonic motor (Shensei USR 60-N4, Japan) was used to rotate the inner cylinder. Like a stepper motor, its revolution can be precisely controlled; the Shensei motor can be rotated in increments of 0.09°. The motor has no magnetic components and can be used in the core of the MRI magnet. However, the motor driving and matching circuitry (D4060, Litton-Westrex, Japan) is not MRI safe, and this circuitry was placed outside the magnet room and connected to the motor via a 7-meter coaxial cable. The motor was

switched off during sonications since the powered motor added noise to the MR images. The motor shaft position was tracked with a high-speed rotary encoder (MTL ME30-10000 C, Japan). The rotary encoder provides real-time feedback during inner cylinder rotation. A Microsoft Foundation Class (MFC) based C++ program was developed to control the motor.

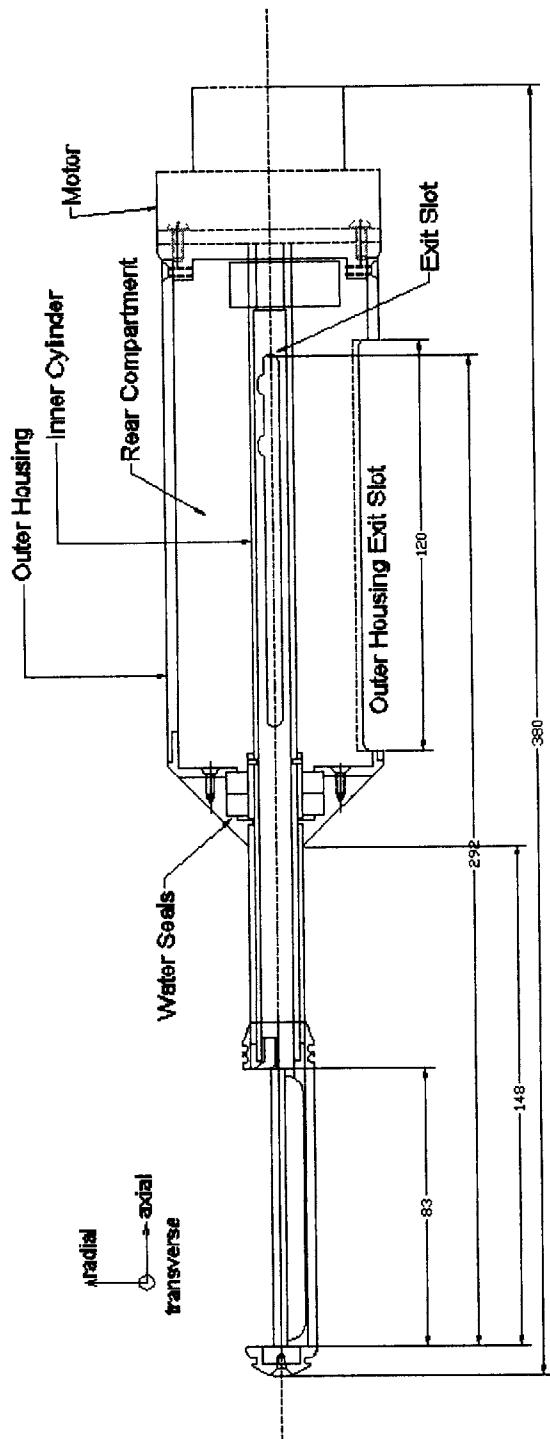


Figure 3-2 . Schematic of the intracavitary applicator. All dimensions are noted in millimeters. The front portion of the applicator hold the transducer. The water lines, air line, and Kapton flex circuit pass through the inner cylinder to the rear compartment and exit the through the slots shown. The rear compartment is protect from water by the water seals. At the rear of the applicator, the motor is attached to the inner cylinder.

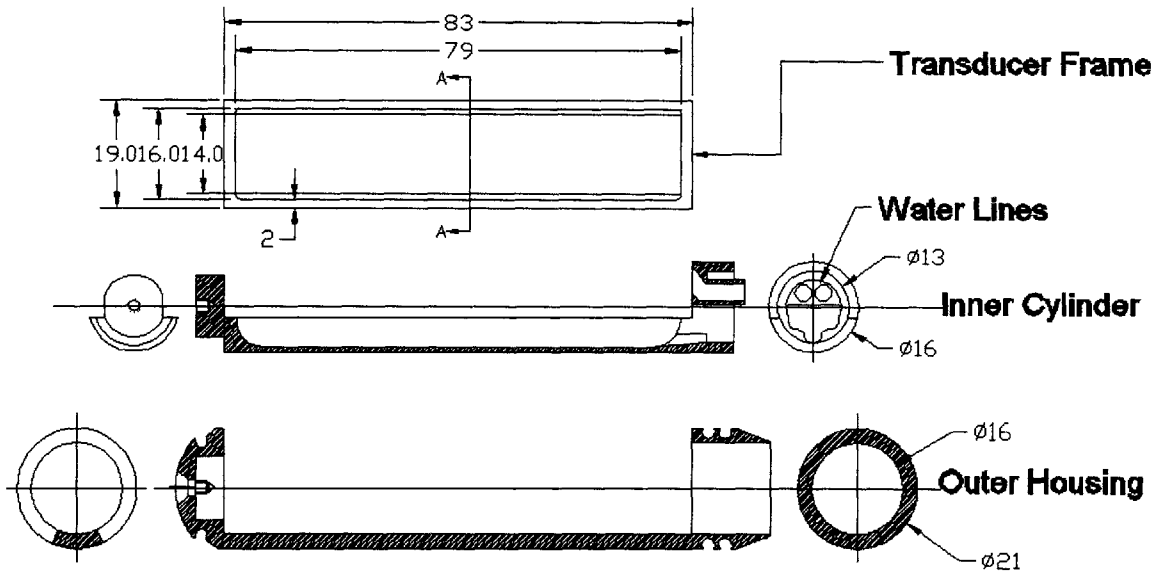


Figure 3-3. Close-up of the front portion of the intracavitary applicator. The Transducer frame holds the linear phased array. The frame is attached to the inner cylinder. The inner cylinder rotates inside the outer housing. The outer housing has O-ring slots for anchoring the latex condom used in the ultrasound coupling system.

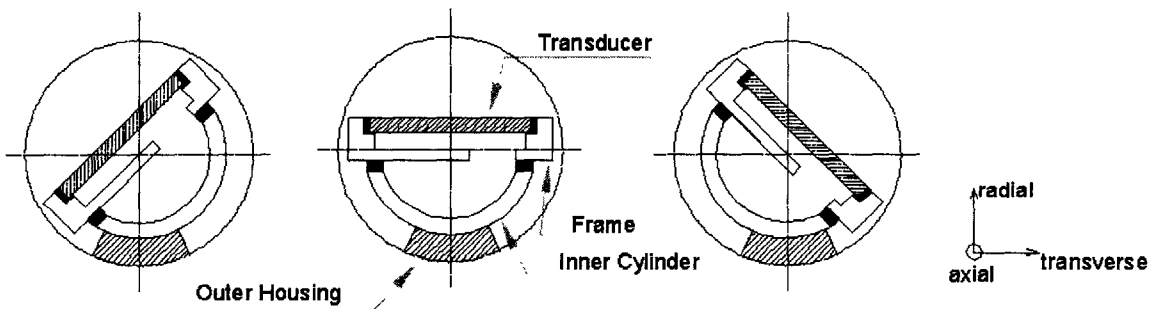


Figure 3-4. Illustration of the array's rotation. The transducer which is mounted in the inner cylinder can rotate 50° in both clockwise and counter-clockwise direction to provide coverage in the transverse axis.

3.3 Assembly & Operation

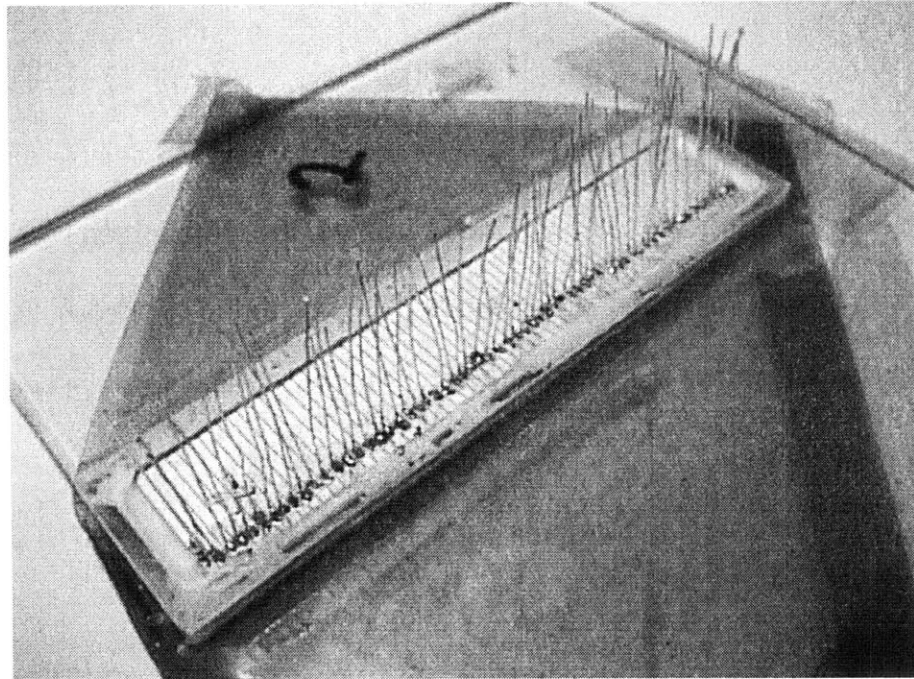
The diced transducer was connected to the flexible circuit and mounted to the intracavitary applicator. Figure 3-5 shows the complete array assembly procedure. First, the diced and filled transducer was mounted in an acrylic frame with VI-SIL V-1022 silicone (Figure 3-5a). Then, 30 AWG single stranded wire-wrap wire was soldered to each element of the phased array (Figure 3-5b). All soldering was done with solder flux at 550 °F. Upon completion of the soldering, the flexible circuit support platform was attached to the frame also with VI-SIL V-1022 silicone (Figure 3-5c). Six pieces of the custom designed Kapton flexible circuit, each piece containing 11 connections, were staggered and glued together with cyanoacrylate adhesive (Liquid Krazy Glue, NY, NY). All solder pads on the flexible circuit were covered with Kapton tape (3M) to protect the pads from any excess adhesive. The layered flexible circuit was threaded through the slot in the rear compartment and pulled out of the open front portion of the application. The Flexible circuit was attached to the platform with double sided tape reinforced with cyanoacrylate (Figure 3-5d). Then, the wires from the array were carefully soldered to the pads of the printed circuit. Once all the wires were attached, the transducer/frame assembly was detached from its glass mount, and the ground plane was soldered to the transmission face of the array using the technique described in the previous section (Figure 3-5e & f). The transducer was then mounted in the applicator using VI-SIL V-1022 and RTV-108 (General Electric). The RTV-108 was used after the VI-SIL V-1022 cured to provide additional waterproofing. Figure 3-6 shows a scaled cross-section view

of the front portion of the applicator with the transducer in place. Note that the transducer is air-backed, and that there is ample room for the Kapton interconnect and all the soldered wires. Air was circulated into the enclosed area behind the transducer to maintain positive pressure.

Following attachment of the transducer, a seven-meter long micro-coaxial cable (Precision Interconnect) assembly (62 wires terminated with a DL connector) was soldered to the opposite end of the flexible circuit in the rear compartment of the applicator. The flexible circuit is L-shaped; the long leg traverses the length of the inner cylinder, and the short leg begins as the printed circuit exits the inner cylinder in the rear compartment. Prior to soldering, the small leg was looped around the inner cylinder once. The connected flex circuit was then anchored in the rear compartment with electrical tape. The anchored loop acts as a strain relief for both the cable assembly and the flexible circuit during inner cylinder rotation. As the motor rotates, the loop tightens in one direction and loosens in the other, preventing tension in the cable and flexible circuit. Figure 3-7 shows this loop and the complete intracavitary applicator with the cable assembly.

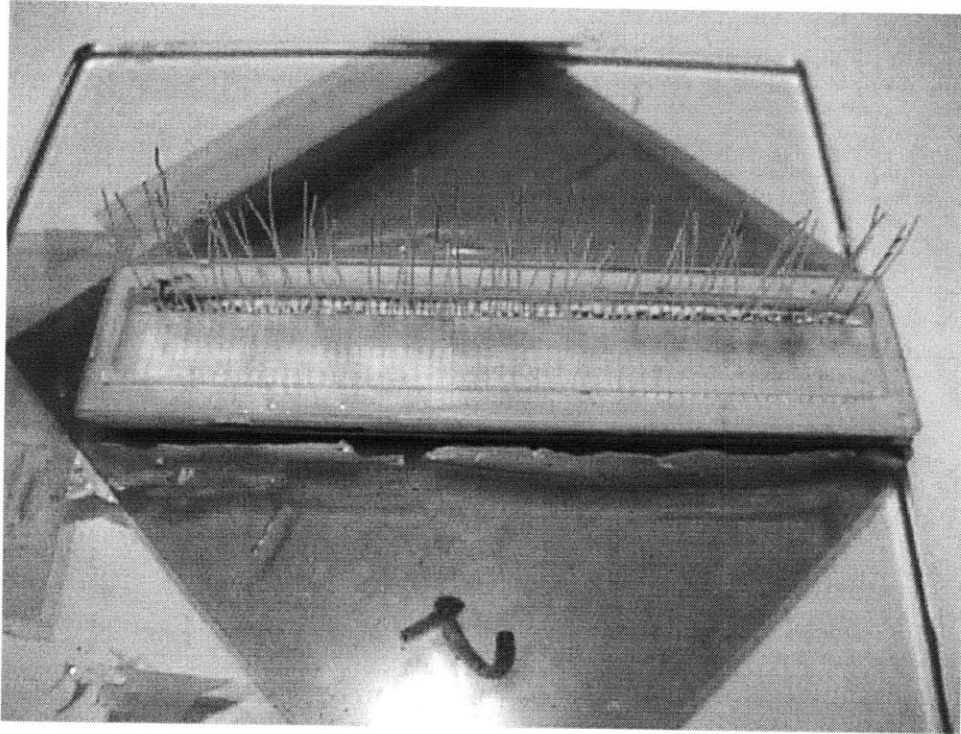


(a)

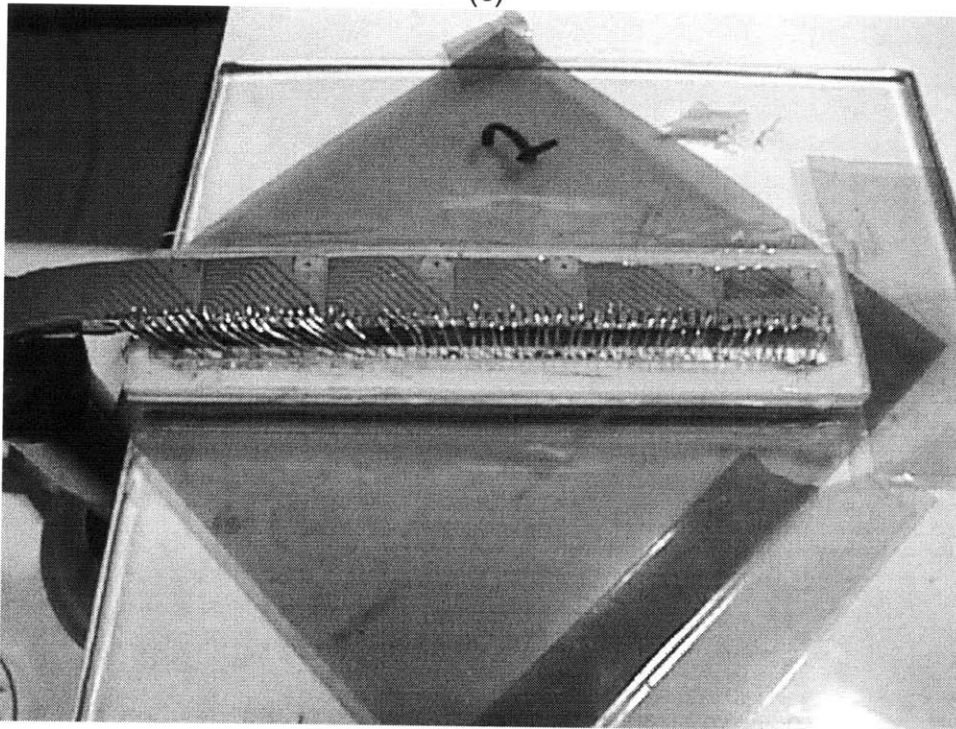


(b)

Figure 3-5. Pictures of the array at various stages of construction. (a) shows the transducer mounted in its frame. (b) shows the wire-wrap wires soldered to the elements.

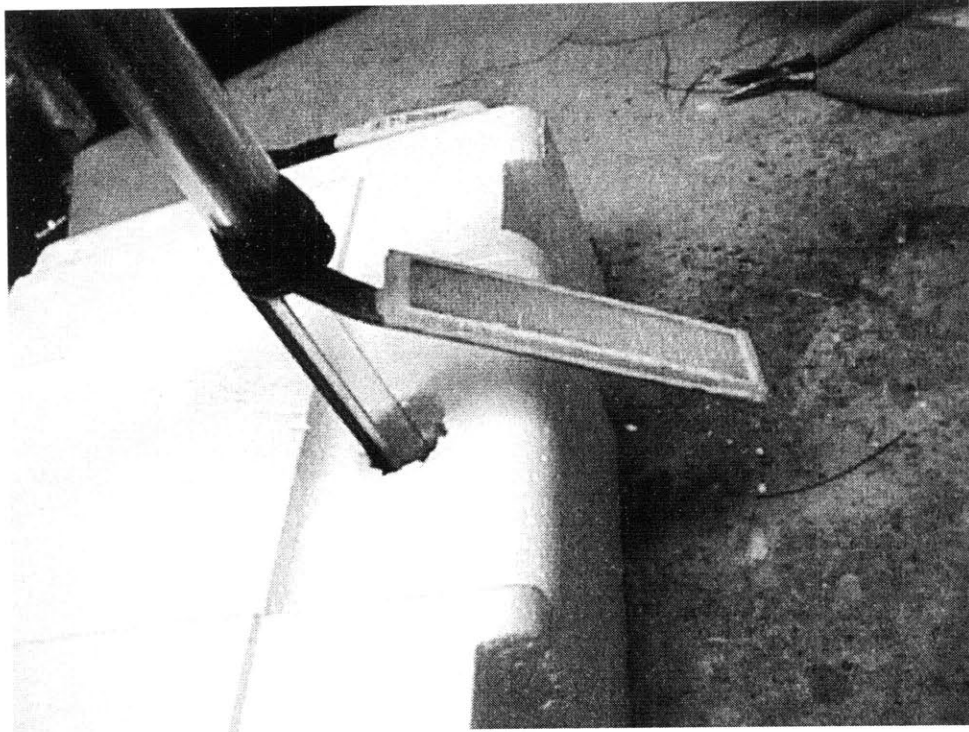


(c)

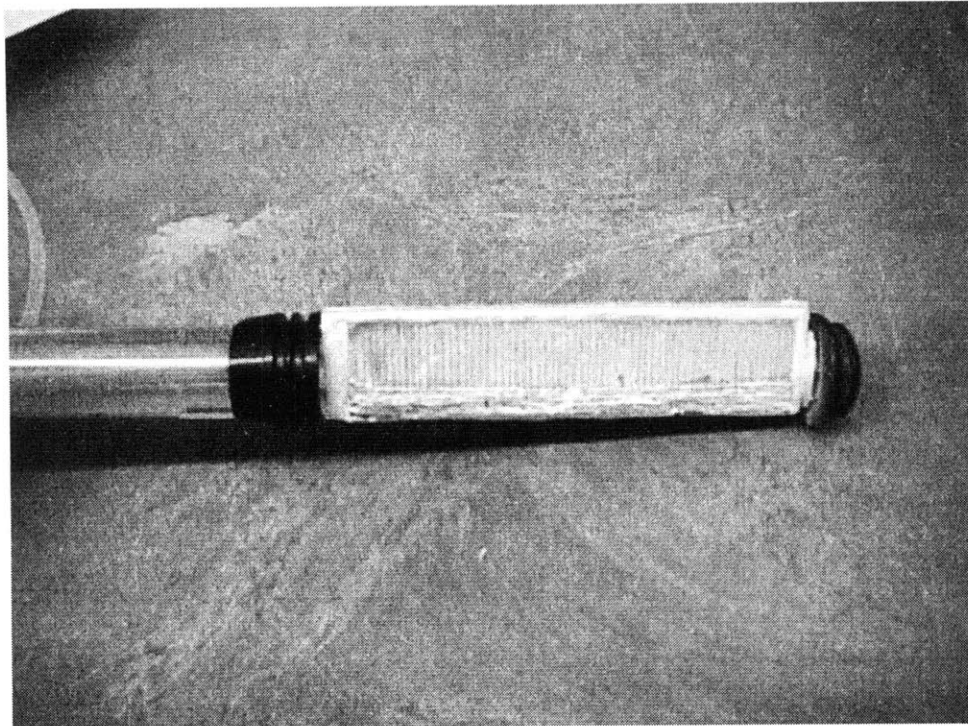


(d)

Figure 3-5. Pictures of the array at various stages of construction. (c) shows the flexible circuit support platform. (d) shows the printed circuit mounted and the connected to the elements of the phased array.



(e)



(f)

Figure 3-5. Pictures of the array at various stages of construction. (e) shows the transducer/frame assembly as it is being mounted in the inner cylinder. (f) shows the finished transducer with ground plane.

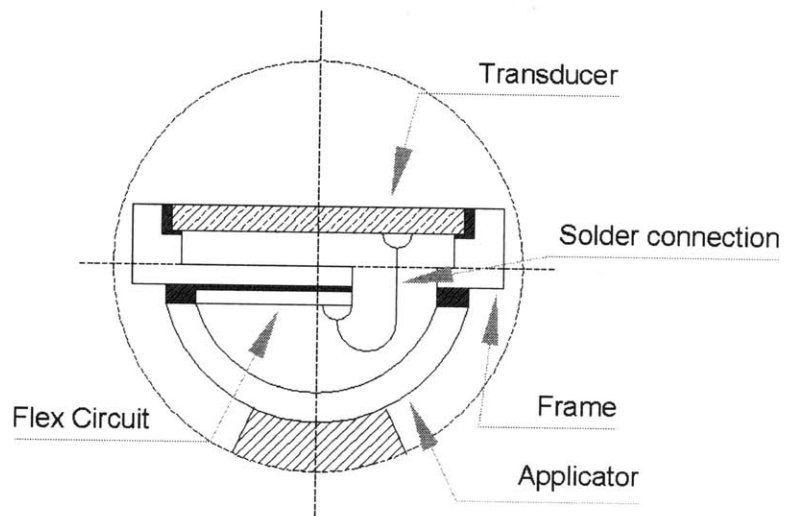


Figure 3-6. Cross-section of the applicator with mounted transducer. All the dark regions in the drawing are regions where adhesives have been used.

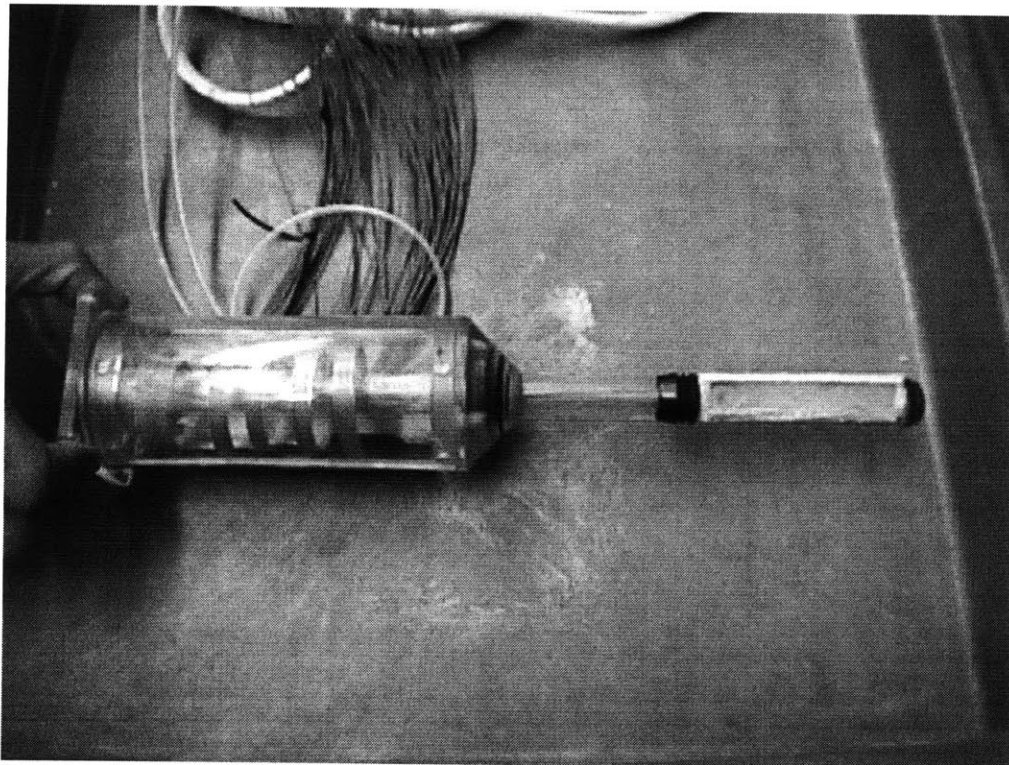


Figure 3-7. Picture of the completed intracavitary applicator. Note the curl in the Kaptan flexible circuit in the rear compartment of the applicator.

3.4 Amplifier

The array is driven by a 64-channel custom designed amplifier system (Daum et al. 1998a). This ultrasound driving system improves the focal intensities of the aperiodic array by up to 25% without the need for implantable hydrophones by incorporating power and phase feedback circuitry. The amplifier is composed of four main blocks: the control system, phase regulation circuitry, power generation circuitry, and matching circuitry. The digital control system takes user input via Microsoft Windows and maintains the specified power and phase setpoints for each element. The driving frequency and other amplifier variables are also set through the control system. The phase regulation block incorporates a phase-locked loop to maintain the set phase at the element. Power is generated with a separate hybrid class D/E power amplifier for each element. The control system, power generation block, and the phase regulation block continuously interact to provide the desired power and phase at the transducer surface. The amplifier is interfaced to the elements of the cabled transducer with an inductor/capacitor matching circuitry used to ensure maximum power transfer.

4 Evaluation of Phased Array in *Ex Vivo* and *In Vivo* Tissues

4.1 Introduction

Two sets of tissue experiments were performed to verify the intracavitary array's capabilities. First, *ex vivo* bovine experiments were performed to demonstrate the three dimensional range of the array. Second, *in vivo* rabbit thigh experiments were used investigate the array's ability to coagulate large tissue volumes. All experiments were performed with MRI guidance and thermometry. The primary goal of this study was to demonstrate the feasibility of MRI-guided ultrasound surgery using an intracavitary phased array.

4.2 Materials and Methods

4.2.1 MRI Experimental Setup

The *ex vivo* specimen or *in vivo* tissue was placed in the bore of a clinical 1.5 Tesla Signa MR imager (GE Medical Systems, Milwaukee, WI). Fresh beef round meat was used in all *ex vivo* experiments to best approximate muscle tissue. For all *in vivo* experiments, ultrasound ablation was performed in thigh muscle of male New Zealand white rabbits. The animals were anesthetized with a mixture of ketamine (48 mg/kg/hr, Fort Dodge Laboratories, Fort Dodge, IA) and xylazine (12 mg/kg/hr, Fermenta Animal Health Co., Kansas City, MO) given as an intra-muscular bolus every hour. The animal's body temperature was constantly monitored with a copper-constantin rectal thermocouple (constructed in-house). The rabbits were provided housing, food, and veterinary care according to NIH

(NIH 1985) and Harvard Medical School guidelines. Ultrasound ablation was performed in both rabbit thighs. To provide an optimal surface for acoustic coupling, the hair from the thighs was removed with an electric shaver and hair removing lotion (Nair, Carter Products, NY, NY).

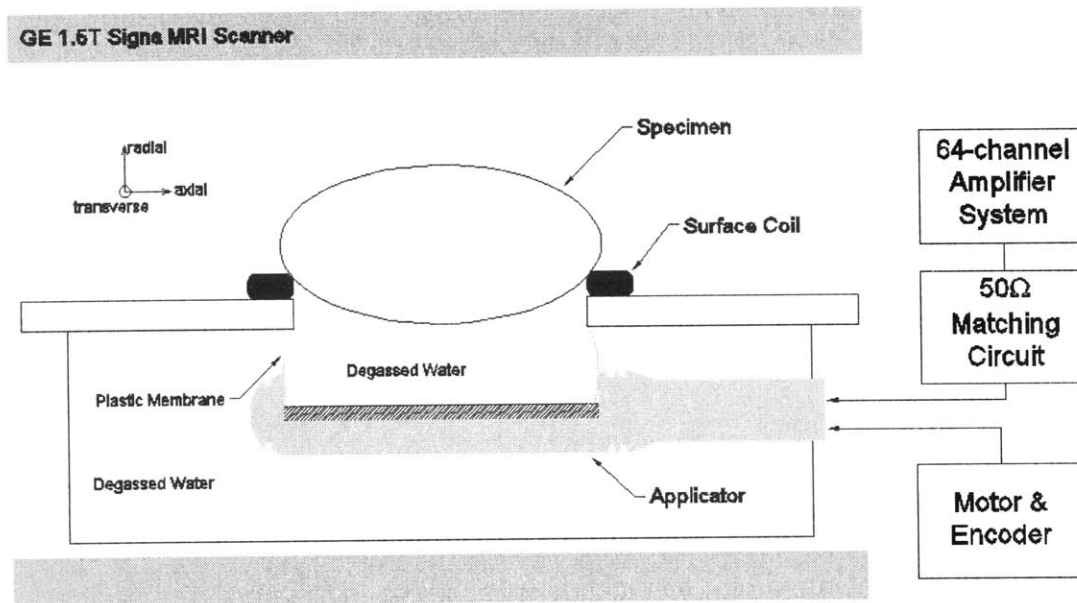


Figure 4-1. Diagram of experimental setup. The intracavitary array was placed in a degassed water bath, and the specimen, phantom or rabbit thigh, was placed directly above the transducer. The MRI surface coil was positioned near the lesion plane to improve image quality.

4.2.2 MRI Imaging Techniques

Through the course of the MRI experiments, three basic MR pulse sequences were used: one sequence to locate the array in relation to the specimen, a temperature sensitive sequence to locate the focus and monitor temperature during ablation, and a third sequence to identify lesions *in situ*.

Prior to sonications, fast spin-echo(FSE) T1-weighted images (TE/TR = 14/500ms, FOV = 20 cm, thickness, echo train length = 4, thickness = 3 mm, matrix size = 256x128, NEX = 2, bandwidth = 16 kHz) were used to position the array with respect to the specimen.

Once the array was properly positioned, temperature images were acquired during a non-destructive low power sonication (25 electrical watts, 20 seconds) to locate the array focus. These temperature images were obtained using the proton chemical shift technique (proton resonant frequency shift constant = 0.00909 ppm/°C; slice thickness = 3 mm, FOV = 16 cm, image acquisition time = 6.0 s, TE/TR = 22.1/45.3 ms, NEX = 1, flip angle = 30°, echo train length = 1, bandwidth = 3.13 kHz). Temperature images were also acquired during the sonication and cooling times. For 20-second sonications, 9 temperature images were obtained over a 60-second period, 3 during the sonication and 6 during the cooling time. For the 30-second sonications, temperature images were also obtained over a 60-second period, but 5 images were acquired during sonication and 4 during cooling.

FSE T2-weighted images (TE/TR = 75/2000ms, echo train length = 8, FOV = 16 cm, thickness = 3 mm, matrix size = 256x256, NEX = 2, bandwidth = 16kHz) were used to identify the focused ultrasound lesions and measure their sizes. Fresh Lesions appear as bright regions in a T2-weighted MRI image, while older lesions appear as dark regions surrounded by a bright ring. Edema can also be detected in the T2-weighted images; it appears as a bright diffuse region and usually surrounds the ultrasound-induced lesion.

4.2.3 Ultrasound Protocols

4.2.3.1 *Ex Vivo* experiments

Ex vivo bovine phantom experiments were performed to demonstrate the phased array applicator's ability to electrically and mechanically move its focus over a large volume. To demonstrate the axial range of the phased array, the focus was electrically moved (by phasing the elements) in 5 mm increments along the long axis of the array at a radial depth of 4 cm. All sonications were done at low power, 25 electrical watts, for 20 seconds. Temperature images were acquired during each sonication to verify the position of the focus. Then, the arrays' ability to create a larger focus in a single sonication was evaluated. Larger foci were created by rapidly switching between three closely spaced focal patterns during a single 30-second sonication. The focal patterns, each a 4 cm-deep focus, were spaced axially at 3 mm increments and scanned at 18 Hz. The large foci generated by the 30-watt sonications were visualized with temperature images. Finally, the transverse range of the phased array was verified by generating 4 cm-deep scanned foci at different motor positions. The transducer was rotated in increments of 15° and low power sonications, 30 watts, were performed for 20 seconds at each position. Again, temperature images were used to visualize the foci.

4.2.3.2 *In vivo* Experiments

In three rabbit thighs, a series of high power 30-second sonications, 130-160 watts each, were used to create large continuous lesions. These lesions were

generated by 8-24 3 cm-deep foci. The constant depth foci were spaced electrically by phasing and mechanically by rotation such that lesions larger than 6 cm³ could be produced. The focus was electrically moved in increments of 3 mm in the axial direction, and the transducer was rotated in increments of 10°. The sonications were separated by at least one minute of cooling time to minimize near-field tissue damage. Following the ablation experiments, the animal was sacrificed and the rabbit thighs were dissected. The ultrasound lesion size was quantified from the gross histology.

4.3 Results

4.3.1 Ex Vivo Experiments

Figure 4-2 is a radial-transverse (RT-plane) T1-weighted MRI image showing the experimental setup. Both the array and the bovine specimen are clearly visible in this image. The two perpendicular lines show the intersection of the other two planes, the axial-transverse (AT) and axial-radial (AR) planes, with the RT image plane. This coordinate system will be used in the subsequent discussions of MRI images.

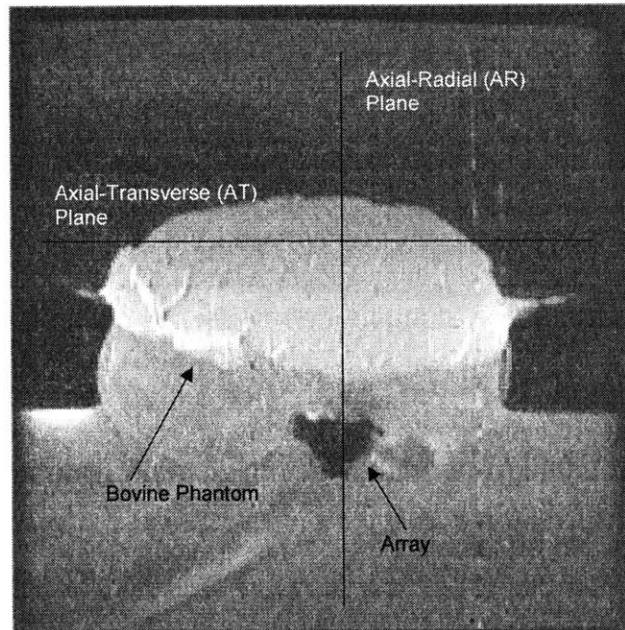


Figure 4-2. T1-weighted radial-transverse (RT) plane image of the bovine phantom setup. The two perpendicular lines show the axial-radial (AR) and axial-transverse (AT) imaging planes.

Figure 4-3 shows the axial range of the transducer. To demonstrate this range, the focus was electrically moved along the long axis of the transducer at a constant radial depth of 4 cm. Figure 4-3a to Figure 4-3f, AT-plane temperature images taken 4 cm from the transducer face, show the focus at -2 cm, -1.5 cm, -1cm, 0 cm, 1cm, and 1.5cm, respectively. Figure 4-3g shows all of these foci superimposed in the same AT-plane image. This image demonstrates that the phased array can cover a 5.5 cm length along its axial dimension. Note that the intensities of the -1 cm, -1.5 cm, and the -2 cm foci are higher than the others. This is due to the array being slightly tilted in the AR-plane. In a series of similar images not shown, the array's focusing ability in the depth dimension was verified to be 3 cm, 2 to 5 cm from the transducer face.

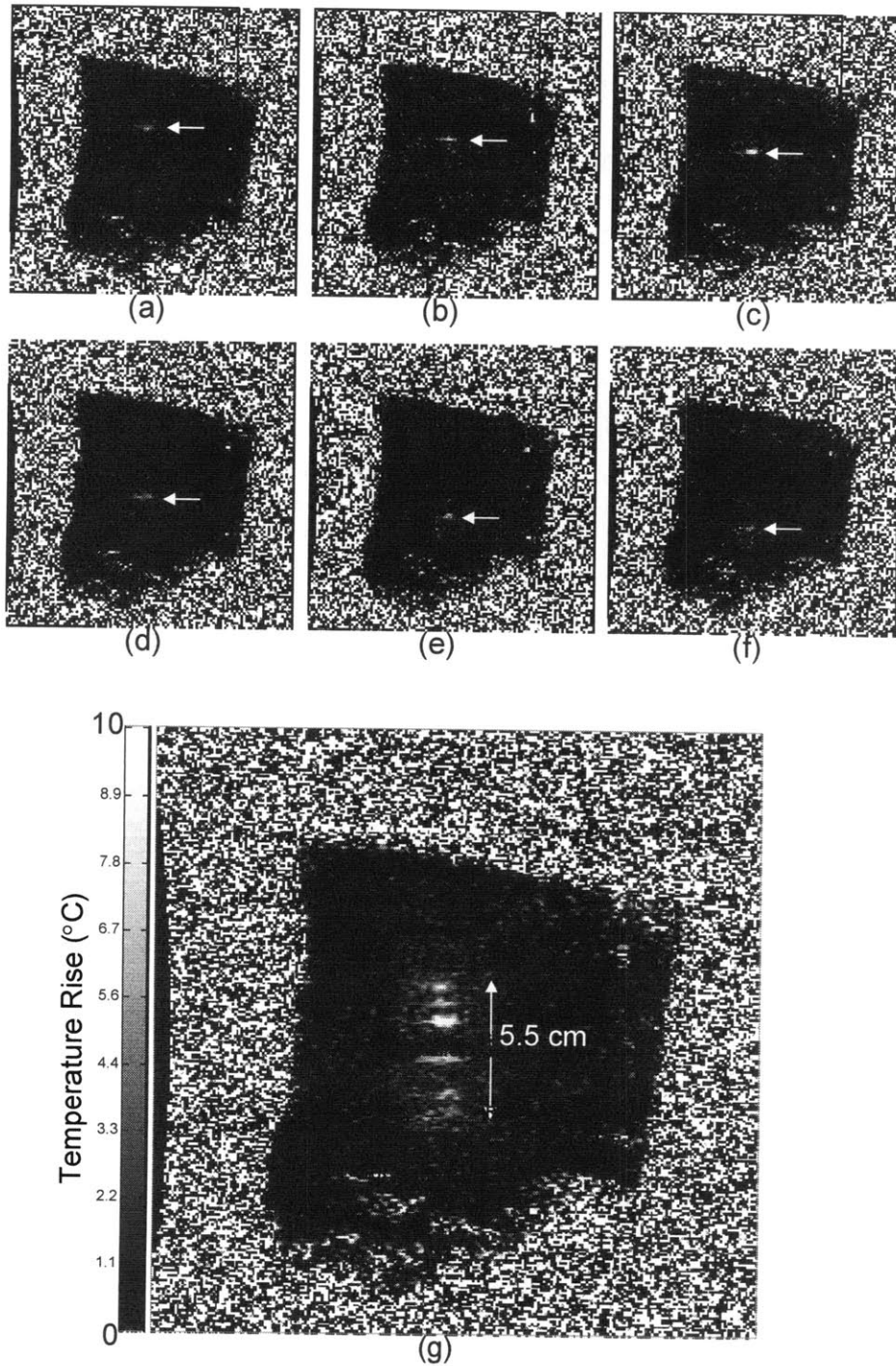


Figure 4-3. AT-plane temperature images showing the phasing abilities of the array. (a)-(f) show the focus as it is moved along the axis of the array. (g) shows all the foci superimposed in one image. The array has a range of 5.5 cm in the axial direction.

Figure 4-4 shows the AT-plane, AR-plane, and RT-plane temperature images of an electrically switched focus. This focus was generated by switching between 3 closely spaced 4-cm deep foci (-3 mm, 0 mm, 3 mm along the axis of the transducer). Note that the scanned focus (Figure 4-4) is almost 3 times larger than the conventional foci (Figure 4-3) in the AT-plane.

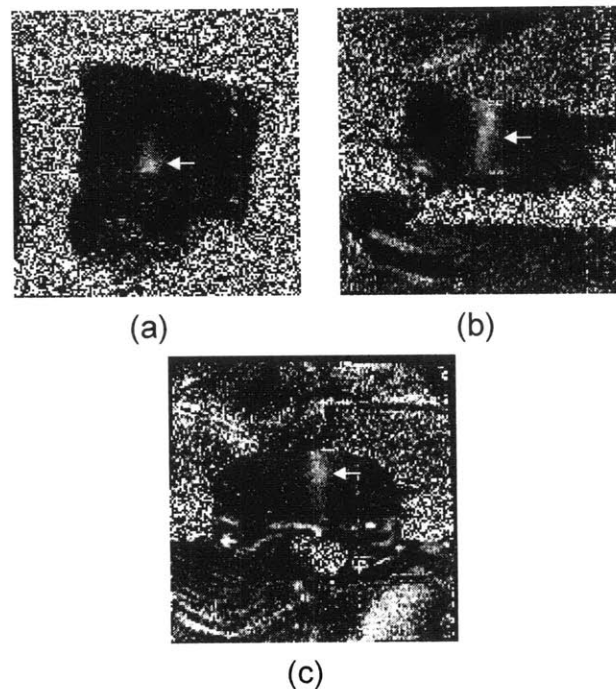


Figure 4-4. AT-plane (a), AR-plane (b), and RT-plane (c) temperature images of a 4 cm-deep focus generated by switching. Arrows show the focus.

Figure 4-5 shows the transverse range of the transducer. To demonstrate this range, a 4cm-deep focus was mechanically rotated in the RT image plane. Figure 4-5a to Figure 4-5e, RT-plane temperature images, show the 4cm-deep focus as the transducer is rotated in increments of 15°. Figure 4-5f depicts all of these foci superimposed in the same RT-plane image. A transverse length of 6 cm can be covered by the applicator via transducer rotation.

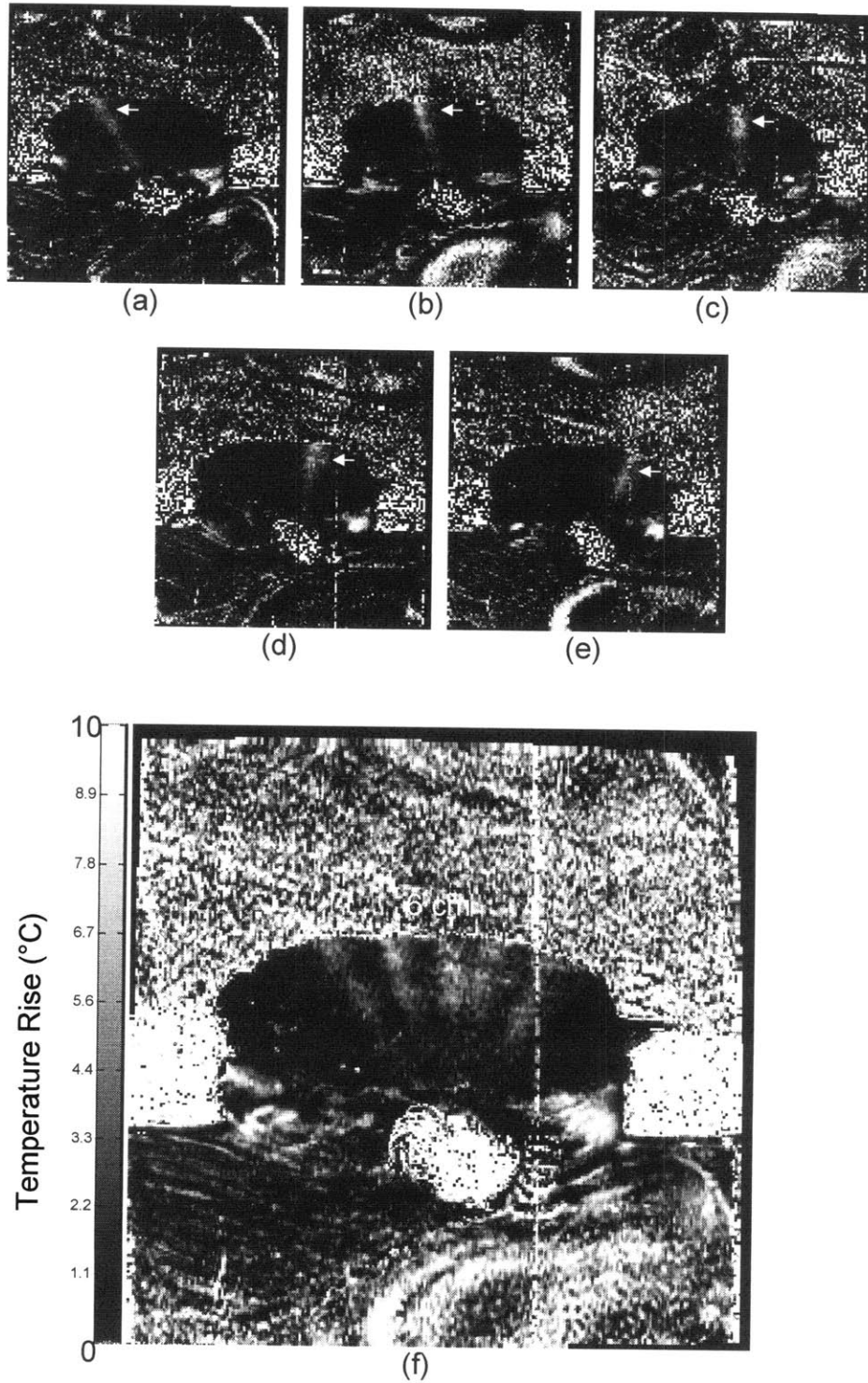


Figure 4-5. RT-plane temperature images showing the transverse focusing range of the array as it is mechanically rotated (arrows show focus). (a)-(f) show the focus at different rotation angles. (g) shows all the foci superimposed in one image. The array has a range of 6 cm in the transverse direction.

4.3.2 *In Vivo* Experiments

MRI temperature images were used to monitor heating during the high power sonications. These images helped to guide sonication spacing. Figure 4-6 shows AR-plane temperature images acquired during and after a 130-watt half-minute sonication. Figure 4-6a shows the whole image plane 5 seconds after the end of sonication (this temperature image can be registered with the T2-weighted image shown in Figure 4-9). Figure 4-6b shows the temperature time course during the 30-second sonication and during 25 seconds of the cooling time. Temperature images acquired during the 30 seconds of sonication were noisy, but still useful in localizing the focus in the tissue. Figure 4-7 shows a plot of the average temperature rise across a 36 mm vertical distance (white line on Figure 4-6a) at the end of sonication. The peak temperature rise of 30°C occurs at the focus. This plot did show negative temperature changes at some points (approximately -2°C maximum). This is within the error of the MR thermometry technique, so the temperature rise was set to 0° C at these points. A plot of the average temperature rise versus time at the focus can be seen in Figure 4-8. The temperature at the focus increases during sonication, and decays immediately after the sonication. The resulting lesion from this single sonication can be seen in Figure 4-9 (indicated by the arrow). The shape and size of the lesion correlates well with the temperature images acquired during the sonication.

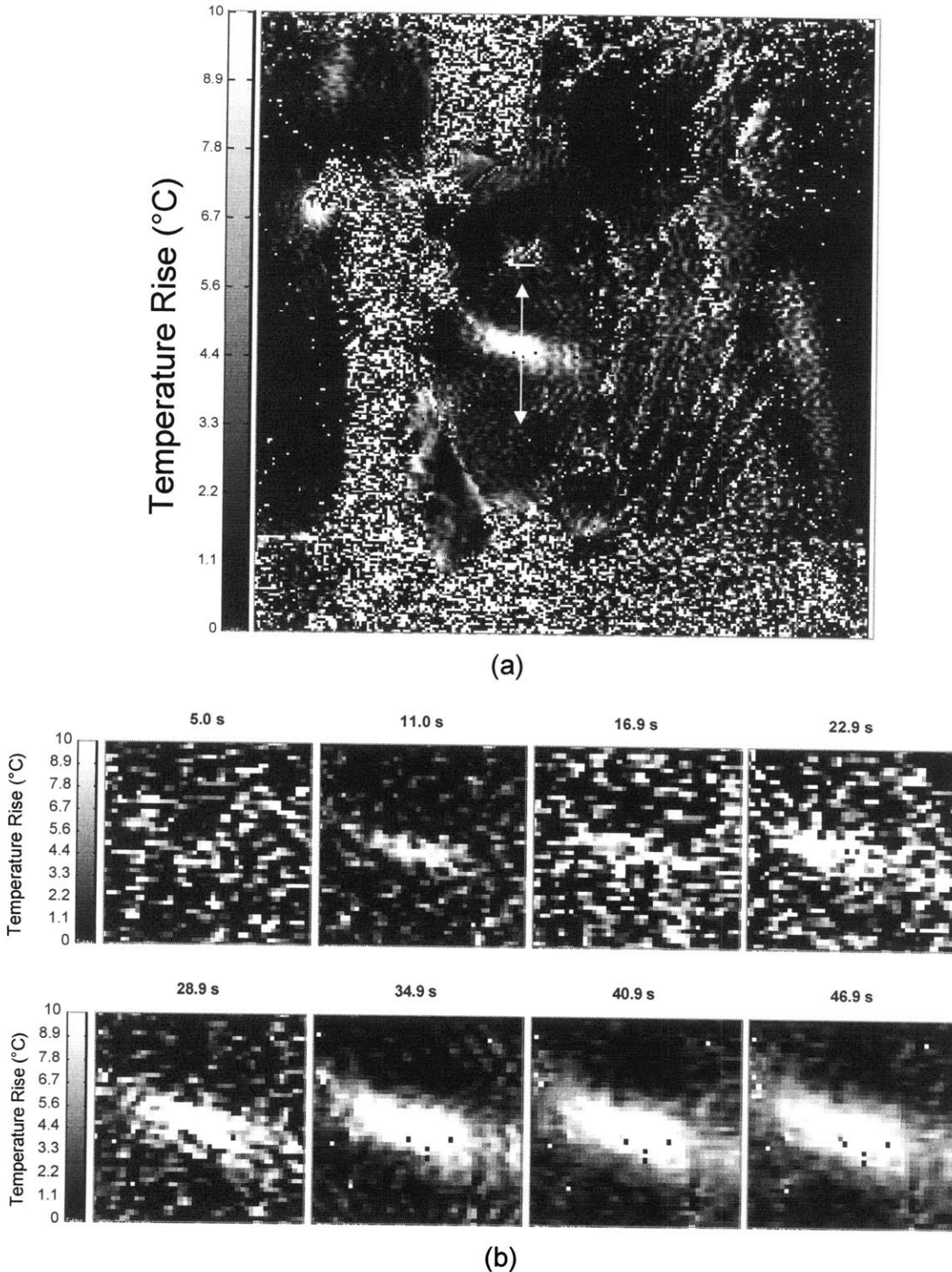


Figure 4-6. AR-plane temperature images acquired during a high power sonication (130 watts, 30 seconds). (a) shows the whole temperature image at 35 second, just after the sonication. (b) shows the temperature time course in the region surrounding the focus. Note that the images acquired during sonication are noisier than the others.

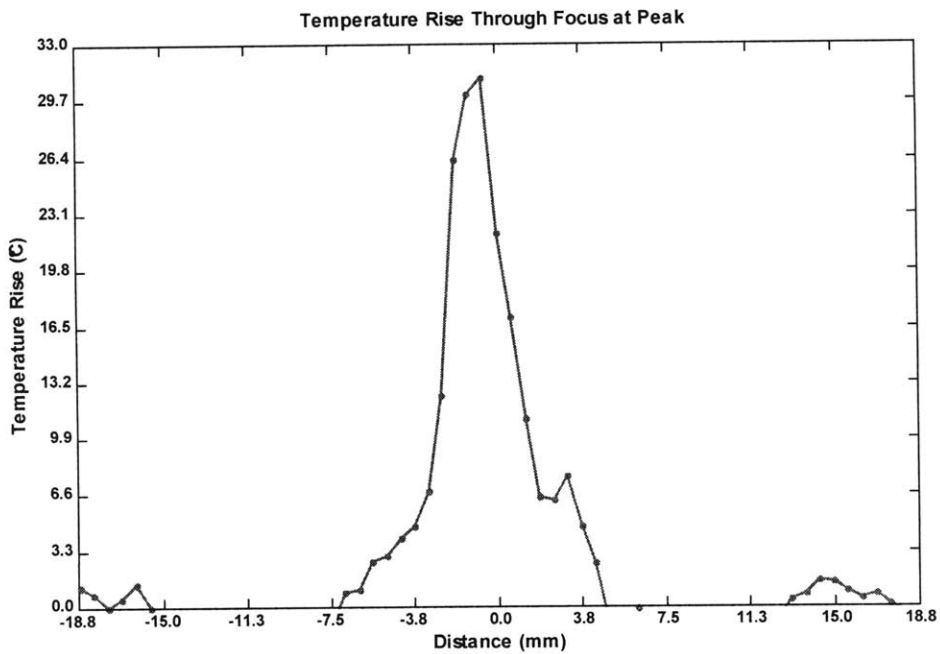


Figure 4-7. Temperature profile along the 36 mm vertical distance shown in Figure 4-6a at the end of sonication. Negative temperature changes have been set to zero.

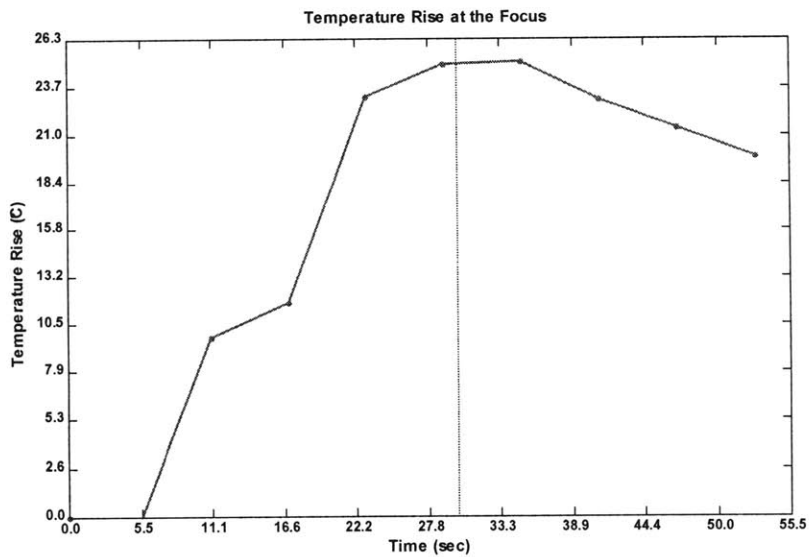


Figure 4-8. Temperature rise at the focus during sonication and during 25 seconds of the cooling time. The end of sonication is marked by the dotted line.

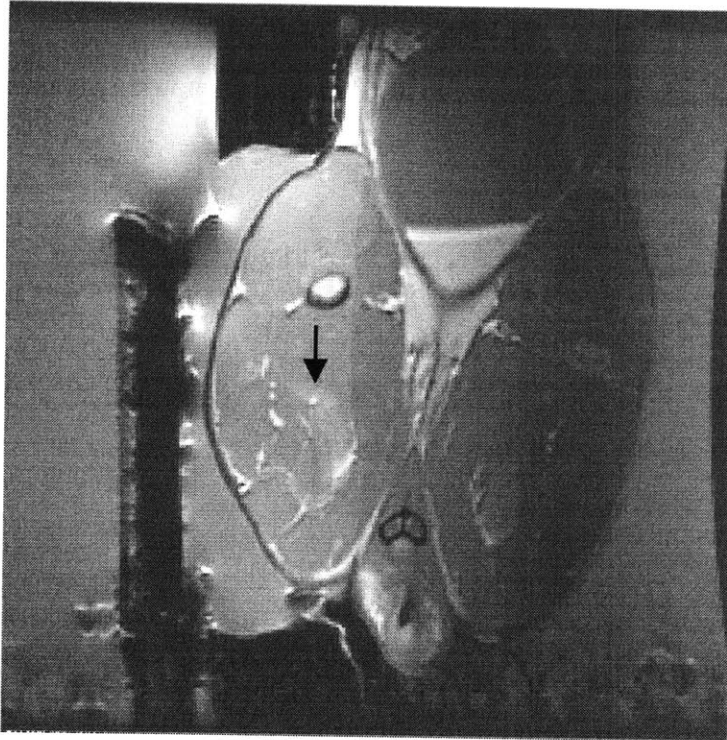


Figure 4-9. T2-weighted image after sonication and cooling. The arrow indicates the lesion created by sonication shown in Figure 4-6.

Three large-volume lesions were created *in vivo* in rabbit thigh muscle. Table 4-1 shows the sonication parameters and the resulting lesion size for each treatment. Lesion size is noted in radial x axial x transverse dimensions. Side effects of each treatment are also listed in the table. Treatment 1 produced the largest lesion, but had the most severe side effects: edema and skin burn. In this treatment, almost every position was sonicated twice. The smallest lesion was created in treatment 2. This treatment consisted of 8 unique 130-watt sonications regularly spaced in the target volume. Treatment 2 had no distinguishable side effects. Treatment 3 consisted of 12 150-watt sonications regular spaced in the target volume. In contrast to the other treatments, each sonication was initiated

immediately after the one minute cooling time. The complete treatment was conducted in less than 20 minutes. Mild edema was noted at the completion of this treatment.

Table 4-1. Outcomes of the three ultrasound in vivo rabbit thigh treatments. The sonication parameters, lesion size, and side effects of each treatment is listed in the table.

Treatment	Sonifications	Lesion Size (depth x length x width)	Side Effects
1	24 sonifications 120-150 watts 30 seconds	4 cm x 3 cm x 3 cm	Edema, skin burn
2	8 sonifications 130 watts 30 seconds	1.5 cm x 2 cm x 2 cm	None
3	12 sonifications 150 watts 30 seconds	3 cm x 2.5 cm x 2 cm	Mild Edema

Figure 4-11 shows AT and AR-plane T2-weighted MRI images of treatment 2 after eight half minute 130-watt sonications. Note that there is no evidence of edema in the post sonication image. The ultrasound-induced lesion is highlighted with the arrows. The lesion measures 1.5 cm x 2 cm in the AT plane and 2 cm x 1.5 cm in this AR image plane. The right lesion boundary in the AT image should not be confused with the neighboring muscle layer, which also has a bright intensity in the image. Figure 4-10 shows the gross histology of the lesion resulting from treatment 2. The MRI-measured lesion size matched the lesion dimensions determined from the histology.

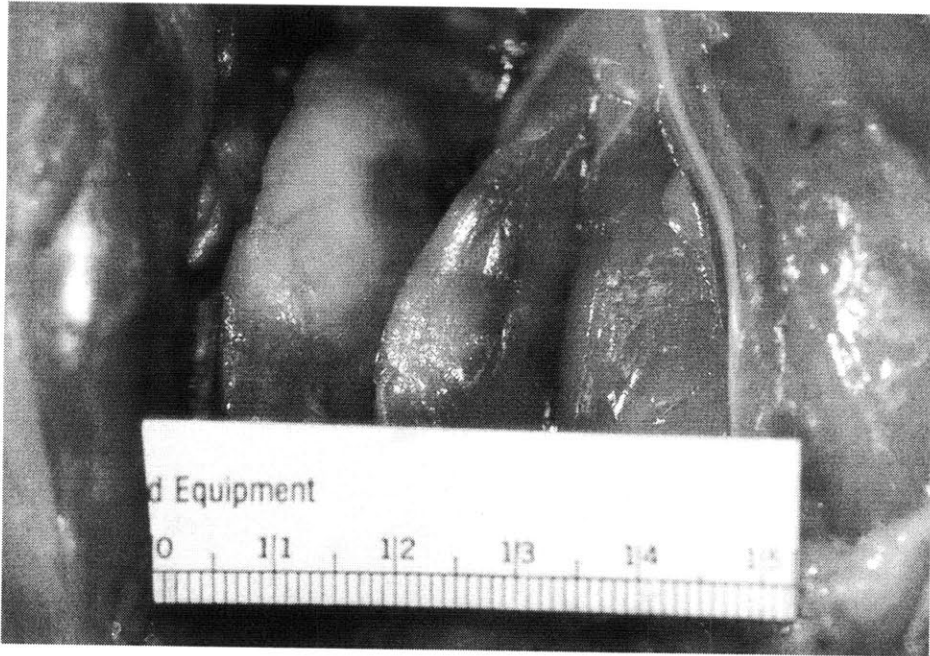
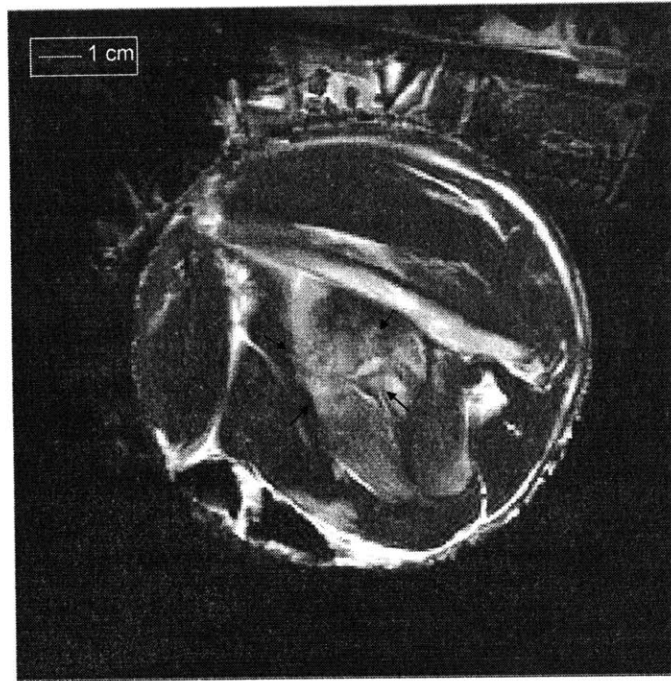
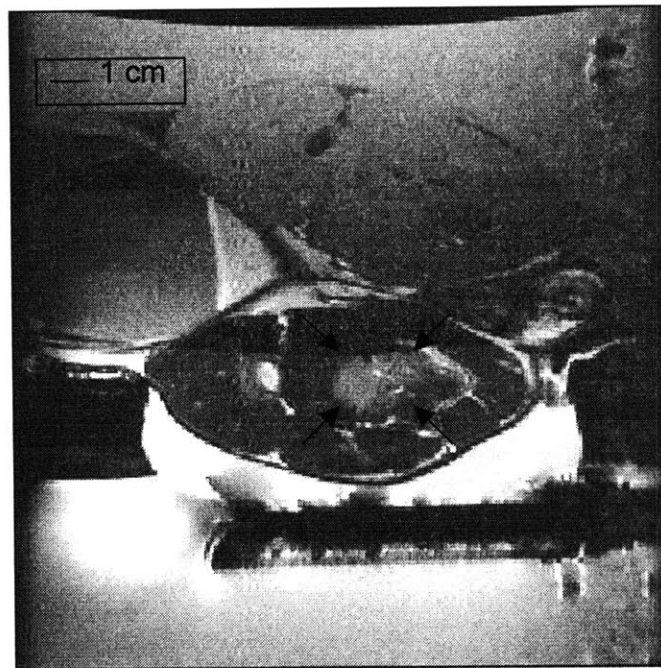


Figure 4-10. Gross histology of treatment 2. The lesion measures 1.5 cm X 2 cm X 2 cm.



(a)



(b)

Figure 4-11. T2-weighted images in the AT-plane (a) and in the AR-plane (b) after 8 sonications (130 watts, 30 seconds). The arrows indicate the ultrasound-induced lesion boundary.

4.4 Discussion

4.4.1 *Ex vivo* Bovine Phantom Experiments

The *ex vivo* studies clearly demonstrated the range of the intracavitary phased array. The results indicate that foci can be created in a volume 5.5 cm x 6 cm x 3 cm (axial x transverse x radial). These dimensions represent an operational maximum and not an absolute maximum volume. Only the center 45 elements of the phased array were powered in the *ex vivo* experiments. If all elements were powered, the 5.5 cm dimension could be extended to at least 6.5 cm. The motor could have been rotated an additional 15° in both directions further increasing the 6 cm transverse range of the applicator. Deeper foci were not created because the phantom extended only 5 cm from the transducer surface. Although a larger volume can be ablated, the operational maximum volume is sufficient to cover the whole human prostate.

The bovine studies were also helpful in treatment planning. The MRI images showed that each sonication created a focus roughly 7 mm x 3 mm x 1.5 cm in size. These dimensions were used in the spacing of the high power sonications in the *in vivo* experiments.

4.4.2 *In vivo* Rabbit Thigh Experiments

The *in vivo* experiments showed that large tissue volumes could be ablated with a linear intracavitary phased array. Furthermore, the number of sonications used to create these large lesions shows potential for a reasonably fast whole prostate ablation treatment. The lesion created in the third treatment represents a

volume half that of the human prostate. Since that treatment was performed in 20 minutes, a volume the size of a human prostate could be ablated in 40 minutes. This treatment time represents a maximum. The duration can be reduced if additional experiments are performed to determine the optimal sonication protocol. Scanned foci, more sparsely spaced foci, or higher power foci may be used to reduce treatment times.

In this study, MRI thermometry helped determine the spacing between successive sonications. However, the temperature images acquired during sonications were noisy. Image corruption during sonication was high due to reflected power in the transducer. For sonications greater than 130 watts, at least 4 watts were reflected. The reflected RF power distorts the RF signals picked up the MR surface coil. If reflected power can be controlled, either by better transducer matching or by deactivating highly reflective elements, better temperature images can be acquired. Improved MR thermometry would then allow for accurate thermal dose maps, and dosage calculations can be directly used to position the multiple sonications involved in one treatment (Chung et al. 1999). A MRI temperature feedback system can be developed which would not only optimize the sonication protocol but also speed up treatment.

The major side effects of large volume ablation were edema and skin burn caused by near field heating. These are serious concerns since these effects would translate into rectal wall heating in prostate treatments. Edema and skin burn were prominent in the first treatment. The cause of near field heating in this treatment was probably due to too many sonications within a targeted volume with

too short interval between the sonications. The first treatment used twice the number of sonications as the third treatment, yet the sonications covered the same volume. The third treatment had no skin burn and only mild edema. Further experiments need to be performed to determine the best sonication protocol for eliminating near field heating. These side effects could also be caused by high powers. In the treatments that had edema, powers greater than 130 watts were used. Treatment 2, which had no side effects, was performed with 120-watt sonications. In addition, short cooling times could be the cause of near field heating. These times could be extended to minimize thermal dose accumulation in the near field. As in the *ex vivo* experiments, only 45 elements of the array were powered during sonications. Powering all the elements of the phased array may also reduce the amount of heat deposited in the near field.

5 Conclusions and Recommendations for Future Work

This study has demonstrated the feasibility of whole prostate ablation with a linear intracavitary phased array. The constructed array has demonstrated that sufficient powers for large volume ablation could be reliably achieved with an intracavitary linear phased array. The thermal prostatectomy technique could provide a definitive, safe, minimally invasive treatment for BPH, T1 and T2 prostate cancers.

However, steps remain before this technique can be tested in humans. Developing the proper sonication protocols is perhaps the most important step. Further animal studies will help determine the appropriate spacing between lesions, and the sonication powers and times. The optimal solution to this, however, can be achieved by calculating thermal dose from MRI temperature images during sonication. If the MR image noise during sonication can be reduced, then thermal dose can be used to accurately predict the lesion size. Then based on the lesion size estimation, the parameters for the subsequent sonications can be appropriately adjusted. A complete MRI temperature feedback system could be developed where the only user input is to determine the volume to be coagulated.

While the treatment planning is being developed, the array geometry could be modified to reduce the near field heating problems. One way to do this is reduce element widths down to $\lambda/2$, this geometry would give us maximum flexibility in focusing while reducing lobe structure. Another geometry that can be

studied is to introduce a curvature to the linear array to add a geometric gain.

This geometry might minimize the heat deposit in the near field. These geometries can be studied with acoustic field simulations prior to array fabrication.

Although advancements were made in fabrication, some work in improving the construction and performance of the array remains. Waterproofing still remains an issue, initial experiments with this array were unsuccessful due to leaking. In addition although the ground plane was robust, this too can be improved to obtain some gain in acoustic efficiency. But more importantly, a better ground plane might reduce the noise generated by reflected powers. Some new ideas for ground plane improvement include: replating the electrode after dicing and filling, using silver impregnated silicone to connect the ground electrodes of all the elements, constructing a piezocomposite array that does not need to be diced.

This technique must be tested in animal prostate models. Creating large lesions in muscle shows feasibility, but some issues remain when attempting to ablate large prostate volumes. First, the level of rectal wall heating with this array needs to be investigated. Second, the ability to ablate prostate tissue immediately adjacent to the rectal wall needs to be verified. If these organ-specific issues along with the aforementioned technical issues can be worked out, then whole prostate ablation with intracavitary ultrasound can become a key treatment option for both BPH and prostate cancer patients.

REFERENCES

- NIH publication no. 85-23. Guide for the care and use of laboratory animals. 1985. Bethesda, MD, U.S. Department of Health and Human Services, Public Health Service, National Institutes of Health.
- Anson KM, Watson GM, Shah TK, Barnes DG. Laser prostatectomy: our initial experience of a technique in evolution. *J Endourol* 1993 Aug; 7:333-336.
- Arrighi HM, Guess HA, Metter EJ, Fozard JL. Symptoms and signs of prostatism as risk factors for prostatectomy. *Prostate* 1990; 16:253-261.
- Bechtold M, Granz B, Heindel HP, Newerla K. 1997. A linear phased array for prostate therapy. 1997 IEEE Ultrasonics Symposium Proceedings. An International Symposium (Cat.No.97CH36118.) :1385
- Benkeser PJ, Frizzell LA, Ocheltree KB, Cain CA. A tapered phased array ultrasound transducer for hyperthermia treatment. *IEEE Trans Ultrason Ferroelectr Freq Contr* 1987; 34:446-453.
- Berry SJ, Coffey DS, Walsh PC. The development of human benign prostate hyperplasia with age. *J Urol* 1994; 151:474.
- Buchanan MT, Hynynen K. The design and evaluation of an intracavitary ultrasound phased array for hyperthermia. *IEEE Trans Biomed Eng* 1994; 41:1178-1187.
- Burov AK. High intensity ultrasonic oscillations for the treatment of malignant tumors in animal and man. *Dokl Akad Nauk SSSR* 1956a; 106:239-241.
- Burov AK, Adreevskaya GD. The effect of ultra-acoustic oscillation of high intensity on malignant tumors in animals and man. *Dokl Akad Nauk SSSR* 1956b; 106:445-448.
- Cain CA, Umemura SA. Concentric-ring and sector vortex phased array applicators for ultrasound hyperthermia therapy. *IEEE Trans Microwave Theory Tech* 1986; MTT-34:542-551.
- Chung A, Jolesz FA, Hynynen K. 1999. Thermal dosimetry of a focused ultrasound beam in vivo by magnetic resonance imaging. [Abstract]. *Med.Phys.(USA)* 26(9):1-10.
- Chung AH, Hynynen K, Colucci V, Oshio K, Cline HE, Jolesz FA. Optimization of spoiled gradient-echo phase imaging for in vivo localization of a focused ultrasound beam. *Magn Reson Med* 1996 Nov; 36:745-752.
- Cline HE, Hynynen K, Watkins RD, Adams WJ, Schenck JF, Ettinger RH, Freund WR, Vetro JP, Jolesz FA. A focused ultrasound system for MRI guided ablation. *Radiology* 1995; 194:731-737.
- Crum LA, Hynynen K. Sound Therapy. *Physics World* 1996; 9:28-33.

- Damianou C, Hynynen K, Fan X. Evaluation of accuracy of a theoretical model for predicting the necrosed tissue volume during focused ultrasound surgery. *IEEE Trans Ultrason Ferroelectr Freq Contr* 1995; 42:182-187.
- Daum DR. A Large Scale Phased Array Ultrasound System for NonInvasive Surgery of Deep Seated Tissue. Ph.D. Thesis. Massachusetts Institute of Technology, 1998.
- Daum DR, Buchanan MT, Fjield T, Hynynen K. 1998a. Design and evaluation of a feedback based phased array system for ultrasound surgery. *IEEE Trans.Ultrason.Ferroelectr.Freq.Control.(USA)* 45(2):431
- Daum DR, Hynynen K. 1998b. Thermal dose optimization via temporal switching in ultrasound surgery. *IEEE Trans.Ultrason.Ferroelectr.Freq.Control (USA)* 45(1):208
- Devonec M, Tomera K, Perrin P. Review: transurethral microwave thermotherapy in benign prostatic hyperplasia. *J Endourol* 1993 Jun; 7:255-259.
- Dewey WC, Hopwood LE, Sapareto SA, Gerweck LE. Cellular responses to combinations of hyperthermia and radiation. *Radiology* 1977 May; 123:463-474.
- Diederich CJ, Burdette EC. 1996. Transurethral ultrasound array for prostate thermal therapy: initial studies. *IEEE Trans.Ultrason.Ferroelectr.Freq.Control (USA)* 43(6):1011
- Diederich CJ, Hynynen K. The development of intracavitary ultrasonic applicators for hyperthermia: a design and experimental study. *Med Phys* 1990 Jul; 17:626-634.
- Diederich CJ, Hynynen K. 1991. The feasibility of using electrically focused ultrasound arrays to induce deep hyperthermia via body cavities. *IEEE Trans.Ultrason.Ferroelectr.Freq.Control (USA)* 38(3):207
- Diederich CJ, Stauffer PR. Pre-clinical evaluation of a microwave planar array applicator for superficial hyperthermia. *Int J Hyperthermia* 1993 Mar; 9:227-246.
- Do-Huu JP, Hartemann P. Annular array transducer for deep acoustic hyperthermia. *IEEE Ultrasonics Symp* 1981; 81:705-710.
- Ebbini ES, Umemura SI, Ibbini M, Cain C. A cylindrical- section ultrasound phased array applicator for hyperthermia cancer therapy. *IEEE Trans Ultrason Ferroelectr Freq Contr* 1988; 35:561-572.
- Fallone BG, Moran PR, Podgorsak EB. Noninvasive thermometry with a clinical x-ray CT scanner. *Med Phys* 1982 Sep; 9:715-721.
- Fan X, Hynynen K. Ultrasound surgery using multiple sonications - treatment time considerations. *Ultrasound Med Biol (USA)* 1996; 22:471-482.
- Fenn AJ. An adaptive-focusing algorithm for a microwave planar phased-array hyperthermia system. *The Lincoln Laboratory Journal* 1993; 6:269-286.

- Fjield T, Hynynen K. The Combined Concentric-Ring and Sector-Vortex Phased Array for MRI Guided Ultrasound Surgery. *IEEE Trans Ultrason Ferroelectr Freq Contr* 1997; 44:1157-1167.
- Fosmire H, Hynynen K, Drach GW, Stea B, Swift P, Cassady JR. Feasibility and toxicity of transrectal ultrasound hyperthermia in the treatment of locally advanced adenocarcinoma of the prostate [see comments]. *Int J Radiat Oncol Biol Phys* 1993 May 20; 26:253-259.
- Frizzell LA, Benkeser PJ, Ocheltree KB, Cain CA. Ultrasound phased arrays for hyperthermia treatment. *IEEE Ultrasonics Symp* 1985; 2:931-935.
- Frizzell LA, Linke CA, Carstensen EL, Fridd CW. Thresholds for focal ultrasonic lesions in rabbit kidney, liver and testicle. *IEEE Trans Biomed Eng (USA)* 1977; BME-24:393-396.
- Frohmuller HG, Theiss M. Radical prostatectomy in the management of localized prostate cancer. *Eur J Surg Oncol* 1995 Aug; 21:336-340.
- Fry FJ, Johnson LK. Tumor irradiation with intense ultrasound. *Ultrasound Med Biol (USA)* 1978; 4:337-411.
- Fry WJ. Production of focal destructive lesions in the central nervous system with ultrasound. *J Neurosurg* 1954; 11:471-478.
- Fry WJ. Intracranial anatomy visualized in vivo by ultrasound. *Invest Radiol* 1968; 3:
- Fry WJ, Fry FJ. Fundamental neurological research and human neurosurgery using intense ultrasound. *IRE Trans Med Electron* 1960; ME-7:166-181.
- Garnick MB, Fair WR. Prostate cancer: emerging concepts. Part I [see comments]. *Ann Intern Med* 1996 Jul 15a; 125:118-125.
- Garnick MB, Fair WR. Prostate cancer: emerging concepts. Part II. *Ann Intern Med* 1996 Aug 1b; 125:205-212.
- Garnick MB, Fair WR. Combating prostate cancer. *Sci Am* 1998 Dec; 279:74-83.
- Gelet A, Chapelon JY, Bouvier R, Pangaud C, Lasne Y. Local control of prostate cancer by transrectal high intensity focused ultrasound therapy: preliminary results. *J Urol* 1999 Jan; 161:156-162.
- Hahn GM. Potential for therapy of drugs and hyperthermia. *Cancer Res* 1979; 39:2264-2268.
- Hand JW. Absorbed power distributions from coherent microwave arrays for localized hyperthermia. *IEEE Trans Microwave Theory Tech* 1986; 34:84-84.
- Hand JW, Ebbini E, O'Keeffe D, Israel D, Mohammadtaghi S. 1993. An ultrasound linear array for use in intracavitary applicators for thermotherapy of prostatic diseases. *IEEE 1993 Ultrasonics Symposium Proceedings (Cat.No.93CH3301.-9)* :1225

- Hollander JB, Diokno AC. Prostatism: benign prostatic hyperplasia. *Urol Clin North Am* 1996 Feb; 23:75-86.
- Horvath J. Ultraschallwirkung beim menschlichen sarkom. *Strahlentherapie* 1944; 75:119.
- Hutchinson EB. Intracavitary Ultrasound Phased Arrays for Thermal Therapies. Ph.D. Thesis. Massachusetts Institute of Technology, 1997 Jan.
- Hutchinson EB, Buchanan MT, Hynynen K. Design and optimization of an aperiodic ultrasound phased array for intracavitary prostate thermal therapies. *Med Phys* 1996 May; 23:767-776.
- Hutchinson EB, Hynynen K. Intracavitary ultrasound phased arrays for prostate thermal therapies: MRI compatibility and in vivo testing. *Med Phys* 1998 Dec; 25:2392-2399.
- Hynynen K. Biophysics and Technology of Ultrasound Hyperthermia. [Anonymous]1990.
- Hynynen K. B-scan transrectal ultrasound hyperthermia system for the treatment of prostate. *Biomedical Thermology* 1994; 13:1-14.
- Hynynen K. Focused ultrasound surgery guided by MRI. *Science&Medicine* 1996a; 3:62-71.
- Hynynen K, Chung A, Colucci V, Jolesz FA. Potential adverse effects of high intensity focused ultrasound exposure. *Ultrasound Med Biol (USA)* 1996b; 22:193-201.
- Ishihara Y, Calderon A, Watanabe H, Mori K, Okamoto K, Suzuki T, Sato K, Kuroda K, Nakagawa N, Tsutsumi S. A precise and fast temperature mapping using water proton chemical shift. *Proc SMRM* 1992;4803.
- Jenne JW, Bahner M, Spoo J, Huber P, Rastert R, Simiantonakis I, Lorenz WJ, Debus J. 1997. CT on-line monitoring of HIFU therapy. 1997 IEEE Ultrasonics Symposium Proceedings. An International Symposium (Cat.No.97CH36118.) :1377
- Johnson C. Nonionizing electromagnetic wave effects in biological materials and system. *Proc of the IEEE* 1972; 60:692-718.
- Kaplan. Transurethral electrovaporization of the prostate. [Anonymous] *Urology*. 1993.
- Landis SH, Murray T, Bolden S, Wingo PA. Cancer statistics, 1999 [see comments]. *CA Cancer J Clin* 1999 Jan; 49:8-31, 1.
- Lee ER. Body comformable 15 MHz micro strip array applicators for large surface area hyperthermia. *IEEE Trans Biomed Eng* 1992; 39:470-470.
- Lele PP. Production of deep focal lesions by focused ultrasound - current status. *Ultrasonics* 1967; 5:105-122.
- Lele PP. Hyperthermia by ultrasound. In *Proceedings of the international symposium on cancer therapy by hyperthermia and radiation*1975, 168-178.

- Lele PP. 1977. Threshold and mechanisms of ultrasonic damage to organized animal tissues [Abstract]. Proceedings of a Symposium on Biological effects and characterization of ultrasound sources Rockville, MA(June 1-3):224-39.
- Lynn JG, Zwemer RL, Chick AJ, Miller AE. A new method for the generation and use of focused ultrasound in experimental biology. *J Gen Physiol* 1942; 26:179-193.
- Madersbacher S, Kratzik C, Susani M, Marberger M. Tissue ablation in benign prostatic hyperplasia with high intensity focused ultrasound [see comments]. *J Urol* 1994 Dec; 152:1956-1960.
- Madersbacher S, Pedevilla M, Vingers L, Susani M, Marberger M. Effect of high-intensity focused ultrasound on human prostate cancer in vivo. *Cancer Res* 1995; 55:3346-3351.
- McDannold, Hynynen K, Wolf D, Wolf G, Jolesz F. MRI evaluation of thermal ablation of tumors with focused ultrasound. *J Magn Reson Imaging* 1998 Jan; 8:91-100.
- Nakahara W, Kabayashi R. Biological effects of ultrasound: mechanisms and clinical application. *Japanese Journal of Experimental Medicine* 1934; 12:137.
- Ocheltree KB, Benkeser PJ, Frizzell LA, Cain CA. An Ultrasonic Phased Array Applicator for Hyperthermia. *IEEE Trans Sonics Ultras* 1987; SU-31:526-531.
- Oka M. Surgical application of high-intensity focused ultrasound. *Clin All Round(Jpn)* 1960; 13:1514.
- Overgaard J. The current and potential role of hyperthermia in radiotherapy. *Int J Radiat Oncol Biol Phys* 1989 Mar; 16:535-549.
- Parker DL. Applications on NMR imaging in hyperthermia: an evaluation of the potential for localized tissue heating and noninvasive temperature monitoring. *IEEE Trans Biomed Eng* 1984; 31:161-167.
- Prat F, Centarti M, Sibille A, Fadil A, Henry L, Chapelon JY, Cathignol D. Extracorporeal high-intensity focused ultrasound for VX2 liver tumors in the rabbit. *Hepatology* 1995; 21:832-836.
- Prat F, Chapelon JY, Fadil A, Sibille A, Theilliere Y, Ponchon T, Cathignol D. Focused liver ablation by cavitation in the rabbit: a potential new method of extracorporeal treatment. *Gut* 1994 Mar; 35:395-400.
- Samulski TV, MacFall JR, Zhang Y, Grant W, Charles HC. Noninvasive thermometry using magnetic resonance diffusion imaging: Potential for application in hyperthermic oncology. *Int J Hyperth (UK)* 1992; 8:819-829.
- Sanghvi NT. Role of cavitation during high intensity focused ultrasound treatment of prostate tissue. In Proceedings 16th International Congress on Acoustics and the 135th Meeting of the Acoustic Society of America 1998, 1067-1068.

- Sanghvi NT, Foster RS, Bihle R, Casey R, Uchida T, Phillips MH, Syrus J, Zaitsev AV, Marich KW, Fry FJ. Noninvasive surgery of prostate tissue by high intensity focused ultrasound: an updated report. *Eur J Ultrasound* 1999 Mar; 9:19-29.
- Sanghvi NT, Fry FJ, Bihle R, Foster RS, Phillips MH, Syrus J, Zaitsev AV, Hennige CW. 1996. Noninvasive surgery of prostate tissue by high-intensity focused ultrasound. *IEEE Trans.Ultrason.Ferroelectr.Freq.Control (USA)* 43(6):1099
- Sheljaskov T, Lerch R, Fuchs A, Schatzle U. 1997. A phased array antenna for simultaneous thermotherapy and sonography. 1997 *IEEE Ultrasonics Symposium Proceedings.An International Symposium (Cat.No.97CH36118.)* :1701
- Short JG. Physical hyperthermia and cancer therapy. *Proc of the IEEE* 1980; 68:133-142.
- Skolnik MI. *Introduction to Radar Systems*. NY, NY 1980.
- Somer JC. Electronic sector scanning for ultrasonic diagnosis. *Ultrasonics* 1968 Jul; 6:153-159.
- Stawarz B, Szmigielski S, Ogronik J, Astrahan M, Petrovich Z. A comparison of transurethral and transrectal microwave hyperthermia in poor surgical risk benign prostatic hyperplasia patients [see comments]. *J Urol* 1991 Aug; 146:353-357.
- Stepanow B, Huber P, Brix G, Debus J, Bader R, van Kaick G, Lorenz WJ. Fast MRI temperature monitoring: Application in focused ultrasound therapy of malignant tissue in vivo. *Proc SMR 3rd Meeting, ISSN 1065-9889* 1995;1172.
- Stewart HF. Ultrasonic Measurement Techniques and Equipment Output Levels. In: Repacholi MH, Benwell DA, eds. *Essentials of Medical Ultrasound: A Practical Introduction to the Principles, Techniques, and Biomedical Applications*. Clifton, NJ: Humana Press. 1982.
- Stoner E. Three-year safety and efficacy data on the use of finasteride in the treatment of benign prostatic hyperplasia. *Urology* 1994 Mar; 43:284-292.
- Strobehn JW. Hyperthermia and cancer therapy: a review of biomedical engineering contributions and challenges. *IEEE Trans Biomed Eng* 1984; 31:779-785.
- Strohmaier WL, Bichler KH, Bocking A, Fluchter SH. Histological effects of local microwave hyperthermia in prostatic cancer. *Int J Hyperthermia* 1991 Jan; 7:27-33.
- Szent-Gorgyi A. Chemical and biological effects of ultrasonic radiation. *Nature* 1933; 131:278.
- ter Haar G. Ultrasound focal beam surgery. *Ultrasound Med Biol* 1995; 21:1089-1100.
- Thurstone FL, von Ramm OT. Electronic beam steering for ultrasonic imaging. In: deVlieger M, ed. *Ultrasound in Medicine*. New York: American Elsevier Publishing. 1974.

Vallancien G, Chartier-Kastler E, Bataille N, Chopin D, Harouni M, Bougaran J. Focused extracorporeal pyrotherapy. *Eur Urol* 1993; 23:48-52.

Wells PNT. *Biomedical Ultrasonics*. Boston: Academic Press. 1977.

5230-26